Science of the Total Environment 917 (2024) 170406

Contents lists available at ScienceDirect

Science of the Total Environment

journal homepage: www.elsevier.com/locate/scitotenv

Impact of particulate nitrate photolysis on air quality over the Northern Hemisphere

Golam Sarwar [a,*], Christian Hogrefe [a], Barron H. Henderson [b], Rohit Mathur [a], Robert Gilliam [a], Anna B. Callaghan [c], James Lee [c], Lucy J. Carpenter [c]

[a] Center for Environmental Measurement & Modeling, U.S. Environmental Protection Agency, Research Triangle Park, NC 27711, USA
[b] Office of Air Quality Planning and Standards, U.S. Environmental Protection Agency, Research Triangle Park, NC 27711, USA
[c] Wolfson Atmospheric Chemistry Laboratories (WACL), Department of Chemistry, University of York, Heslington, York YO10 5DD, UK

HIGHLIGHTS

- Particulate nitrate photolysis enhances nitrogen dioxide, nitrous acid, and ozone.
- Particulate nitrate photolysis initiates ozone peaks in spring.
- Particulate nitrate photolysis produces more ozone than lost due to halogen chemistry.
- Dimethyl sulfide chemistry reduces the impact of particulate nitrate photolysis on ozone.

GRAPHICAL ABSTRACT

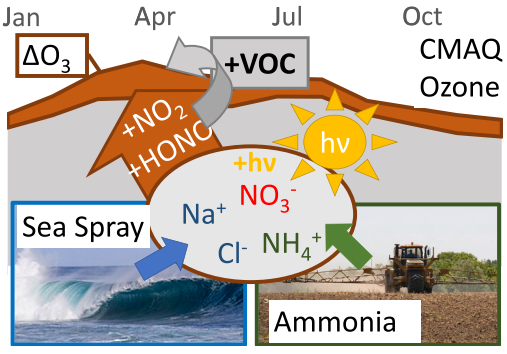

ARTICLE INFO

Editor: Hai Guo

Keywords:
Particulate nitrate
Photolysis
HONO
NO_2
O_3

ABSTRACT

We use the Community Multiscale Air Quality (CMAQv5.4) model to examine the potential impact of particulate nitrate (pNO_3^-) photolysis on air quality over the Northern Hemisphere. We estimate the photolysis frequency of pNO_3^- by scaling the photolysis frequency of nitric acid (HNO_3) with an enhancement factor that varies between 10 and 100 depending on pNO_3^- and sea-salt aerosol concentrations and then perform CMAQ simulations without and with pNO_3^- photolysis to quantify the range of impacts on tropospheric composition. The photolysis of pNO_3^- produces gaseous nitrous acid (HONO) and nitrogen dioxide (NO_2) over seawater thereby increasing atmospheric HONO and NO_2 mixing ratios. HONO subsequently undergoes photolysis, producing hydroxyl radicals (OH). The increase in NO_2 and OH alters atmospheric chemistry and enhances the atmospheric ozone (O_3) mixing ratio over seawater, which is subsequently transported to downwind continental regions. Seasonal mean model O_3 vertical column densities without pNO_3^- photolysis are lower than the Ozone Monitoring Instrument (OMI) retrievals, while the column densities with the pNO_3^- photolysis agree better with the OMI retrievals of tropospheric O_3 burden. We compare model O_3 mixing ratios with available surface observed data from the U.S., Japan, the Tropospheric Ozone Assessment Report – Phase II, and OpenAQ; and find that the model without pNO_3^- photolysis underestimates the observed data in winter and spring seasons and the model with pNO_3^- photolysis improves the comparison in both seasons, largely rectifying the pronounced underestimation in spring.

* Corresponding author at: US EPA, 109 T.W. Alexander Drive, Research Triangle Park, NC 27711, USA.
E-mail address: sarwar.golam@epa.gov (G. Sarwar).

https://doi.org/10.1016/j.scitotenv.2024.170406
Received 21 November 2023; Received in revised form 8 January 2024; Accepted 22 January 2024
Available online 26 January 2024

Compared to measurements from the western U.S., model O_3 mixing ratios with pNO_3^- photolysis agree better with observed data in all months due to the persistent underestimation of O_3 without pNO_3^- photolysis. Compared to the ozonesonde measurements, model O_3 mixing ratios with pNO_3^- photolysis also agree better with observed data than the model O_3 without pNO_3^- photolysis.

1. Introduction

Atmospheric processing of nitrogen oxides (NO_x) produces nitric acid (HNO_3), which partitions into particulate nitrate (pNO_3^-). While the slow photolysis of HNO_3 can return some NO_x to the atmosphere, pNO_3^- is thought to be the end reaction product, which can only be removed from the atmosphere via dry and wet deposition. Thus, pNO_3^- has traditionally been considered a permanent sink for NO_x. However, recent field and experimental studies challenge this traditional view by suggesting that pNO_3^- can undergo photolysis to produce nitrous acid (HONO) and nitrogen dioxide (NO_2) with potentially important implications for air quality. Gen et al. (2022) and Cao et al. (2023) completed comprehensive reviews of pNO_3^- photolysis in the atmosphere and reported the details of the mechanism and factors affecting the photolysis. pNO_3^- absorbs UV light under atmospherically relevant condition and transforms into an excited state which can then decompose to nitrite or react to form NO_2. Nitrite can then undergo further reaction producing HONO. Ye et al. (2016) measured gaseous and aerosol species during an aircraft campaign over the North Atlantic in July of 2013, and reported elevated HONO mixing ratios and pNO_3^- concentrations in the remote marine atmosphere. They found HONO and pNO_3^- were correlated and suggested that pNO_3^- photolysis produces HONO with a photolysis frequency ~ 300 times faster than that of HNO_3. They used measured chemical species and known atmospheric chemistry and predicted atmospheric HONO mixing ratios using a box model. Their predicted HONO mixing ratios were much lower than the observed HONO data over the clean marine environment. When they introduced the photolysis of pNO_3^-, the model successfully reproduced the observed HONO mixing ratios. To further support their suggestion, they collected ambient aerosol samples, performed laboratory chamber experiments, and detected HONO and NO_2 from the photolysis of pNO_3^-.

Reed et al. (2017) reported measurements of NO_x at the Cape Verde Atmospheric Observatory (CVAO) (16° 51′ 49 N, 24° 52′ 02 W) and noted that NO_x mixing ratios peak at around noon. Their box model without photolysis of pNO_3^- did not reproduce the observed diurnal pattern of NO_x. However, the addition of pNO_3^- photolysis in the box model (with HONO and NO_2 yields as shown in Eq. (1)) helped reproduce the observed NO_x diurnal cycle and was able to explain the observed HONO data at CVAO.

$$pNO_3^- \xrightarrow{h\nu} 0.67 \times HONO + 0.33 \times NO_2 \quad (1)$$

Ye et al. (2017) collected aerosol samples near the ground surface from urban, suburban, and remote areas of New York in 2008–2010 and aloft using an aircraft in the southeast U.S. in the summer of 2013. HONO and NO_2 were detected in chamber experiments when the collected aerosol samples were exposed to ultraviolet light, but not when the light was turned off. Ye et al. (2017) concluded that photolysis of pNO_3^- produces HONO and NO_2 and reported a mean pNO_3^- photolysis frequency greater than ~87 times that of HNO_3. The results also suggested that chemical composition, including organic matter and nitrate loading, can affect photolysis frequency. Additional experiments reported by Bao et al. (2018) show that aerosol samples from urban areas of Beijing, China that were exposed to a xenon lamp in a photochemical flow reactor also produced HONO and NO_2 only when the light was turned on and showed HONO formation to be correlated with pNO_3^-. These authors reported that pNO_3^- photolysis frequencies 1–3 orders of magnitude higher than that of HNO_3 and suggested that the photochemical aging of pNO_3^- is an important atmospheric HONO production pathway in Beijing, China. Shi et al. (2021) performed laboratory photolysis experiments in a Teflon chamber using particulate sodium and ammonium nitrate. They also suggested that the photolysis of pNO_3^- can release HONO and NO_2. They, however, reported a pNO_3^- photolysis frequency of <10 times faster than that of HNO_3 and suggested that pNO_3^- photolysis plays a limited role in air quality.

Ye et al. (2018) further reported the measurements of HONO and other relevant chemical species using an aircraft in the southeastern U.S. during the summer of 2013. The daytime mean HONO mixing ratio was 11.2 pptv in the planetary boundary layer and 5.6 pptv in the free troposphere. Ye et al. (2018) calculated a daytime mean HONO source of 53 pptv hr^{-1}, suggesting that nearly 70 % of HONO was produced from the pNO_3^- photolysis, and reported a pNO_3^- photolysis frequency of $2.0 \times 10^{-4}\ s^{-1}$ compared to the value of $7.0 \times 10^{-7}\ s^{-1}$ for HNO_3 photolysis at a solar zenith angle of 0^0. Conversely, Romer et al. (2018) analyzed NO_x and HNO_3 data over the Yellow Sea measured during the 2016 Korea−United States Air Quality (KORUS-AQ) Study and found that rapid pNO_3^- photolysis was not consistent with their measurements. These authors suggested that pNO_3^- photolysis can only occur at a frequency of 1–30 times faster than that of HNO_3.

Zhu et al. (2022) reported HONO and NO_x measurements during the 2019 spring and summer at the Tudor Hill Marine Atmospheric Observatory in Bermuda. They reported higher mixing ratios of HONO and NOx in polluted plumes and suggested that NO_x reactions were the dominant source for daytime formation of HONO. In the clean marine atmosphere with low NO_x, they reported a distinct HONO diurnal cycle with a peak occurring around noon and lower values at night. Zhu et al. (2022) suggested that NO_x reactions contributed to ~21 % of the daytime HONO source while the pNO_3^- photolysis accounted for the remaining daytime HONO source with an enhancement factor of 29 for pNO_3^- photolysis compared to that of HNO_3. Andersen et al. (2023) reported HONO measurements at surface and aloft using an aircraft near CVAO and provided strong evidence that pNO_3^- photolysis enhances daytime HONO, with a photolysis frequency that increases with relative humidity and decreases with pNO_3^- concentrations. The average enhancement factor for pNO_3^- photolysis compared to that of HNO_3 in this study was 70. Their results mostly reconcile the large discrepancies in pNO_3^- photolysis frequencies reported in previous field and laboratory studies.

Kasibhatla et al. (2018) implemented photolysis of coarse mode sea-salt pNO_3^- into the GEOS-Chem model with $4^0 \times 5^0$ horizontal grid-resolution and compared model predictions with measurements at the CVAO. They reported that sea-salt pNO_3^- photolysis frequencies of 25–50 times greater than that of HNO_3 reproduces the observed NO_x data. HONO prediction with the photolysis of pNO_3^- reproduced the diurnal pattern of observed HONO but under-predicted the daytime observed peak data. Their analysis suggests that the upper limit of pNO_3^- photolysis frequency can be ~100 times greater than that of HNO_3. They reported that the global tropospheric impacts of the (coarse mode only) sea-salt pNO_3^- photolysis on NO_x, O_3, and OH are relatively small (1–3 %). They performed a sensitivity analysis by also including photolysis of accumulation-mode pNO_3^- and reported 1–2 ppbv (parts per billion by volume) O_3 increase over most regions and > 6 ppbv increase over northern India and eastern China. Zhang et al. (2022) added six HONO sources in the WRF-Chem model, performed simulations over North China, and compared model predictions with measurements of HONO, O_3, and other chemical species. The six HONO sources included traffic emissions, soil emissions, indoor emissions, NO_2 heterogeneous reaction

on aerosol, NO_2 heterogeneous reaction on ground, and pNO_3^- photolysis with a photolysis frequency of 30 times the HNO_3 photolysis frequency. The model without the additional HONO sources failed to capture the observed HONO data but the model with the additional sources reproduced observed HONO data and increased O_3 and fine particles. They completed additional sensitivity simulations using pNO_3^- photolysis frequency of 1, 7, 30, and 120 times the HNO_3 photolysis frequency and analyzed the resulting model predictions. They reported that selecting a larger value of the pNO_3^- photolysis frequency may cover up other ground based unknown HONO sources but overestimate vertical sources of HONO as well as NO_x and O_3, and emphasized the need for additional studies to determine the exact pNO_3^- photolysis frequency in the atmosphere.

Shah et al. (2023) compared four atmospheric models including GEOS-Chem to observations from three aircraft campaigns including the Atmospheric Tomography Mission (ATom). They used the GEOS-Chem model with $4^\circ \times 5^\circ$ horizontal grid-resolution to perform an annual simulation for 2015 and selected months in 2012, 2013, 2016, 2017, and 2018; and reported that GEOS-Chem underestimates nitric oxide (NO) observations over the Pacific and Atlantic oceans and suggested the existence of a missing source. They were able to account for the missing source by adding the pNO_3^- photolysis. The photolysis frequency of pNO_3^- was expressed using an enhancement factor (EF) which indicates how fast it occurs relative to that of HNO_3 and proposed the following equation for EF:

$$EF = 100 \times max\left(\frac{[SSA]}{[SSA] + [pNO_3^-]}, 0.1\right) \quad (2)$$

where [SSA] is the molar concentration of sea-salt and $[pNO_3^-]$ is the molar concentration of pNO_3^-.

Previous studies (Ye et al., 2017, 2018; Bao et al., 2018; Andersen et al., 2023) suggest that the photolysis frequency of pNO_3^- is higher over the clean marine environment and lower over pNO_3^- rich atmospheres (Romer et al., 2018; Shi et al., 2021). Eq. (2) produces a maximum of 100 and a minimum of 10 for EF. The addition of pNO_3^- photolysis in the GEOS-Chem model increased O_3 mixing ratios by up to 5 ppbv and improved the low model bias compared to the ozonesonde measurements. It also increased the global tropospheric OH mixing ratios by 19 %.

Dang et al. (2023) used the GEOS-Chem model with $4^\circ \times 5^\circ$ horizontal grid-resolution over the globe and $0.5^0 \times 0.625^0$ grid-resolution over North America and performed model simulations for 2009 and 2017 to understand the sources and trends of background NO_2 over the contiguous U.S. The model without pNO_3^- photolysis underestimated NO_2 vertical column densities compared to the retrievals from the Ozone Monitoring Instrument (OMI). Including pNO_3^- photolysis, with the same enhancement factor of Shah et al. (2023), increased NO_2 column densities by 13 % annually and improved comparisons with OMI data. Here, we examine the potential impact of modeled pNO_3^- photolysis on air quality using the Community Multiscale Air Quality (CMAQv5.4) model (www.epa.gov/cmaq), a widely used air quality model in regulatory analysis and air quality research in many countries (Appel et al., 2021; Kitayama et al., 2019; Mathur et al., 2022) that does not currently include pNO_3^- photolysis.

2. Methodology

2.1. Model description

CMAQ contains comprehensive treatments of atmospheric emissions, transport, gas-phase chemistry, aerosols, cloud processes, dry and wet deposition. We use the CMAQ model configured for the Northern Hemisphere with a horizontal resolution of 108 km and 44 vertical layers (Mathur et al., 2017). We use the Weather Research and Forecasting (WRFv4.3.3) (Skamarock, 2008) model for generating meteorological fields and the Meteorological-Chemistry Interface Processor (MCIPv5.3.3) for preparing model-ready meteorology needed for the CMAQv5.4 model. We compare WRF predicted precipitation, temperature, wind speed, and water vapor mixing ratio to available observed data in the U.S. and compute Mean Absolute Error (MAE), Root Mean Squat Error (RMSE), Mean Bias (MB) and Correlation Coefficient (r) for each month (Table S.1). Gilliam et al. (2021) previously compared WRF predictions for 12-km Contiguous U.S (CONUS) and 108-km Northern Hemisphere domains for 2002–2019 with observed data over the CONUS. Error, bias and correlation shown in Table S.1 for the 108-km Northern Hemisphere domain are consistent to those shown by Gilliam et al. (2021) and represent reasonable model performance considering the coarser grid-resolution. The domain and configuration used in this study was identical to those used in the EPA's Air QUAlity TimE Series (EQUATES) (https://www.epa.gov/cmaq/equates) (Foley et al., 2023) except the use of lightning assimilation used here.

Foley et al. (2023) describe the anthropogenic and fire emissions over the U.S., Canada, and Mexico which we use in this study. We use anthropogenic emissions over China from the Tsinghua University and anthropogenic emissions for all other regions from the Hemispheric Transport of Air Pollution (HTAPv2) (Janssens-Maenhout et al., 2015) with scaling factors derived from the Community Emissions Data System (Hoesly et al., 2018). Fire emissions are from the Fire Inventory from the National Center for Atmospheric Research (FINN) version 1.5 (Wiedinmyer et al., 2011) for outside North America, Biogenic Volatile Organic Carbon (VOC) and soil nitric oxide (NO) emissions are from version 2.1 of global emissions from the Copernicus Atmosphere Monitoring Service (CAMS) (Sindelarova et al., 2014), and lightning NO emissions are from the Global Emissions InitiAtive (GEIA) monthly climatology (Price et al., 1997).

For gas-phase chemistry, we use the Carbon Bond chemical mechanism version 5 (CB6r5) (Yarwood et al., 2020) augmented with detailed chlorine (Sarwar et al., 2012), bromine and iodine chemistry (CB6r5m) (Sarwar et al., 2019). CMAQv5.4 contains detailed treatments of elemental carbon (EC), organic carbon (OC), non-carbon organic mass (NCOM), sulfate (pSO_4^{2-}), nitrate (pNO_3^-), ammonium (pNH_4^+), unspeciated particles (OTHER), trace elements, and secondary organic aerosols species (Binkowski and Roselle, 2003; Murphy et al., 2017). CMAQ contains sea-spray emissions from the ocean (Gantt et al., 2015) and wind-blown dust emissions. Sea-spray emissions in CMAQ are speciated into 7 aerosol species (Millero, 1996) while wind-blown dust emissions are speciated into 28 aerosol species using U.S. EPA's SPECIATE database (Simon et al., 2010) including pNO_3^- with a mass fraction of 0.00002 (gm/g). Sea-spray emissions are not speciated into pNO_3^-. CMAQ uses ISORROPIA II for calculating partitioning of total nitrate between HNO_3 and pNO_3^- (Fountoukis and Nenes, 2007).

CB6r5m contains photolysis of 68 gaseous compounds including HNO_3 and uses absorption and quantum yield data from the International Union of Pure and Applied Chemistry (IUPAC) to calculate photolysis frequencies of HNO_3 (Atkinson et al., 2004). However, it does not include photolysis of pNO_3^-. We add the fine mode pNO_3^- photolysis reaction (Eq. (1)) to CMAQv5.4 using the Shah et al. (2023) proposed expression (Eq. (2)) for calculating EF. We multiply the photolysis frequency of HNO_3, calculated at each timestep, by EF to estimate the photolysis frequency of pNO_3^-. We do not use coarse mode pNO_3^- photolysis in this study. Unlike GEOS-Chem, CMAQ does not separately track sea-salt concentrations as a unique species. Instead, the sea-spray emissions are speciated into other aerosol species. For this study, we tracked sea-salt concentration by adding an additional tracer species for sea-salt in CMAQ.

We performed two annual simulations for 2018. Each simulation was initiated on October 1, 2017, and continued through December 31, 2018. The first 3 months were used as spin-up and the results covering the entirety of 2018 were analyzed and presented subsequently. Initial

conditions for both simulations were obtained from a previous simulation (the EPA's Air QUAlity TimE Series (EQUATES)) (https://www.epa.gov/cmaq/equates). Boundary conditions for both simulations are identical and discussed in Mathur et al. (2017). One simulation uses the CB6r5m without the photolysis of pNO_3^- while the other simulation uses CB6r5m with the photolysis of pNO_3^-. Differences in the results between the two simulations are attributed to the photolysis of pNO_3^-. To better understand the importance of the chemistry in different emissions scenarios, we performed several additional model sensitivity simulations for January 2018. Each of these simulations was also conducted with a 3-month spin-up time (October 1–December 31, 2017). Additional details of these simulations are described in Section 4.

Mean model calculated photolysis frequencies of HNO_3 and pNO_3^- (mean over the entire seawater and land areas) are shown in Fig. 1. Photolysis frequencies of HNO_3 over seawater near the surface are similar to those over land. However, photolysis frequencies of HNO_3 over seawater at higher altitudes are slightly greater than those over land. Photolysis frequencies of pNO_3^- over seawater and land are greater than those of HNO_3 and photolysis frequencies of pNO_3^- over seawater are consistently greater than those over land. Our annual mean enhancement factor at surface over land is ~80 and decreases with altitude reaching ~41 at an altitude of ~14 km. In contrast, our annual mean enhancement factor at surface over ocean is ~98 and also decreases with altitude reaching ~63 at the similar altitude. Values over land vary with locations - lower values occur over pNO_3^- rich areas (for example portion of China) but higher values occur over areas adjacent to oceans where sea salt can be transported easily. These enhancement factors, though higher than those reported in Zhang et al. (2021) and Zhang et al. (2022), are consistent with those used in several other recent studies (Shah et al. (2023), Dang et al. (2023), Fu et al. (2019)) and highlight existing uncertainties in pNO_3^- photolysis frequencies and the need for better quantification of its spatial and temporal variability in the troposphere.

2.2. Description of observed data used in model evaluation

We use pNO_3^- measurements from the Interagency Monitoring of PROtected Visual Environments (IMPROVE) (http://vista.cira.colostate.edu/Improve), the Clean Air Status and Trends Network (CASTNET) (www.epa.gov/castnet/download-data), and the Chemical Speciation Network (CSN) (www.epa.gov/amtic/chemical-speciation-network-csn) for model evaluation. For evaluating model NO_2 and O_3 vertical column density, we use data from the OMI satellite retrievals (https://aura.gsfc.nasa.gov/omi.html). We use ozonesonde measurements from the World Ozone and Ultraviolet Radiation Data Centre (WOUDC) (https://woudc.org/home.php) and the National Oceanic and Atmospheric Administration (NOAA) Earth System Research Laboratories (ESRL) (https://gml.noaa.gov/ozwv/ozsondes) for evaluating model predictions aloft.

For evaluating model surface O_3 predictions, we use measurements from the Air Quality System (AQS) (www.epa.gov/aqs), the NOAA ESRL (https://gml.noaa.gov/ozwv/surfoz), Acid Deposition Monitoring Network in East Asia (www.eanet.asia), the Tropospheric Ozone Assessment Report – Phase II (TOAR2) (https://igacproject.org/activities/TOAR/TOAR-II), and OpenAQ sites (https://openaq.org). We use HONO measurements at CVAO in 2015 and 2023. Reed et al. (2017) described the CVAO HONO measurements during November 25–December 3, 2015. The 2023 HONO measurements are described here. HONO was measured at the CVAO during 7th to 26th February 2023 using a long path absorption photometer (LOPAP-03 QUMA Elektronik & Analytik GmbH). The LOPAP measurement technique is described in detail by Heland et al. (2001) and Kleffmann et al. (2002). To summarize, HONO is collected into the liquid phase from the sampled air flow as a diazonium salt through reaction with reagent 1 (100 g sulfanilamide dissolved in 9 L deionized water and 1 L HCl) and is then mixed with reagent 2 (0.8 g n-(1-naphtyl)-ethylenediamine dihydrochloride dissolved in 8 L deionized water) to make an azo-dye. The absorption of the azo dye at 550 nm is measured with a spectrometer and is used to determine the mixing ratio of HONO. The LOPAP has two channels, the first channel measures HONO and interferences, the second channel measures only interferences, allowing an interference-free HONO mixing ratio to be determined. At the CVAO, the LOPAP inlet was placed on the roof of a container lab, with a sampling height of roughly 3 m above ground. The instrument was zeroed with N_2 (N5 purity) every 6 h for 30 min and was calibrated using a Titrisol nitrite standard solution (1000 mg of NO_2^- diluted to 0.01 mg L^{-1}). Three calibrations were performed during the campaign, on 9th, 11th and 21st February. The detection limit was calculated to be 0.3 ppt (2σ), using the noise during zero measurements. The relative error of the instrument

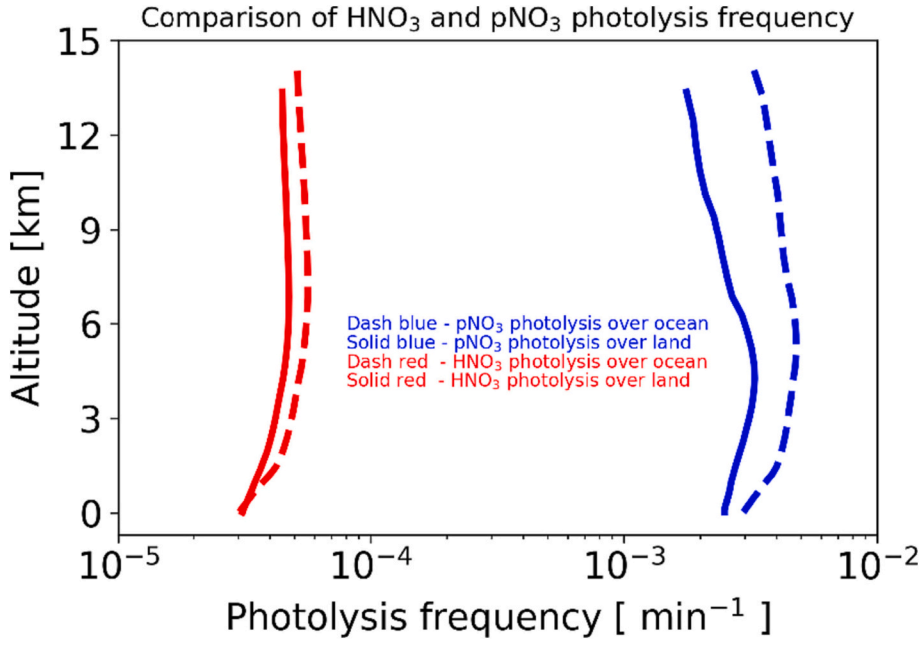

Fig. 1. A comparison of CMAQ calculated photolysis frequencies of HNO_3 and pNO_3^- over seawater and land.

was estimated as 10 % of the measured HONO value.

3. Results

3.1. Impact on annual daytime mean pNO_3^-, NO_2, HONO, and O_3 at different altitudes

Predicted concentrations of pNO_3^- and mixing ratios of NO_2, HONO, and O_3 without and with pNO_3^- photolysis are shown in Fig. 2. The concentrations and mixing ratios at each model vertical layer are averaged separately over all land and ocean areas and are shown as a function of altitude. pNO_3^- concentrations over land with pNO_3^- photolysis are marginally lower than the concentrations without the photolysis at lower altitude (<3 km); however, the concentrations with pNO_3^- photolysis decrease aloft compared to those without photolysis [Fig. 2(a)]. In contrast, pNO_3^- concentrations over the ocean with pNO_3^- photolysis are consistently lower than the concentrations without photolysis due to greater pNO_3^- photolysis frequencies over ocean than land. pNO_3^- photolysis produces HONO and NO_2 and increases their mixing ratios. HONO undergoes photolysis during the day producing OH. The additional OH reacts with NO_2 and produces HNO_3, which partitions to pNO_3^-, compensating for pNO_3^- lost via photolysis. Predicted HONO mixing ratios over land without and with pNO_3^- photolysis are similar near the surface (<1 km), suggesting that the chemistry has only a minor impact near the surface over land [Fig. 2(b)], where alternative sources of HONO such as NO_2 hydrolysis dominate (Finlayson-Pitts and Pitts Jr., 2000). However, mixing ratios aloft with pNO_3^- photolysis are higher than without photolysis. pNO_3^- photolysis consistently increases HONO over the ocean at all altitudes. Impacts on NO_2 mixing ratios over land and ocean are similar to those of HONO [Fig. 2(c)], which is expected as pNO_3^- photolysis directly produces both HONO and NO_2 (R1). Enhancements over seawater are greater than those over land due to higher pNO_3^- photolysis frequencies over seawater. pNO_3^- photolysis has a substantial impact on O_3 and increases mixing ratios over land and ocean at all altitudes [Fig. 2(d)]. Enhanced NO_2 and OH from the photolysis participate in atmospheric chemistry, producing more O_3 over seawater, which is then transported to downwind continental regions resulting in the increased mixing ratios over land from the surface to ~14 km. Percent increases of O_3 due to this chemistry are also shown in the figure. Percent increases in O_3 over the ocean are greater than those over land near the surface (<~4 km) [Fig. 2 (d)], however the relative impacts aloft are similar.

Numerous studies have documented the reduction of O_3 by bromine and iodine chemistry over seawater (Saiz-Lopez et al., 2014; Fernandez et al., 2014; Sarwar et al., 2015; Sherwen et al., 2016; Sarwar et al., 2019; Kang et al., 2021). These studies suggest that bromine and iodine emitted from seawater destroy O_3 near the surface and aloft; however, the reduction is largest near the surface and the extent of the reduction decreases with altitude. Kang et al. (2021) reported that the bromine and iodine chemistry in CMAQ reduces O_3 by ~16 % near the surface. In contrast, the pNO_3^- photolysis increases O_3 by >16 % not only over seawater but also over land near the surface as well as aloft. Thus, pNO_3^- photolysis more than compensates for the O_3 reduction due to the bromine and iodine chemistry.

3.2. Impact on annual daytime mean surface pNO_3^-

Predicted annual mean daytime surface pNO_3^- without the pNO_3^-

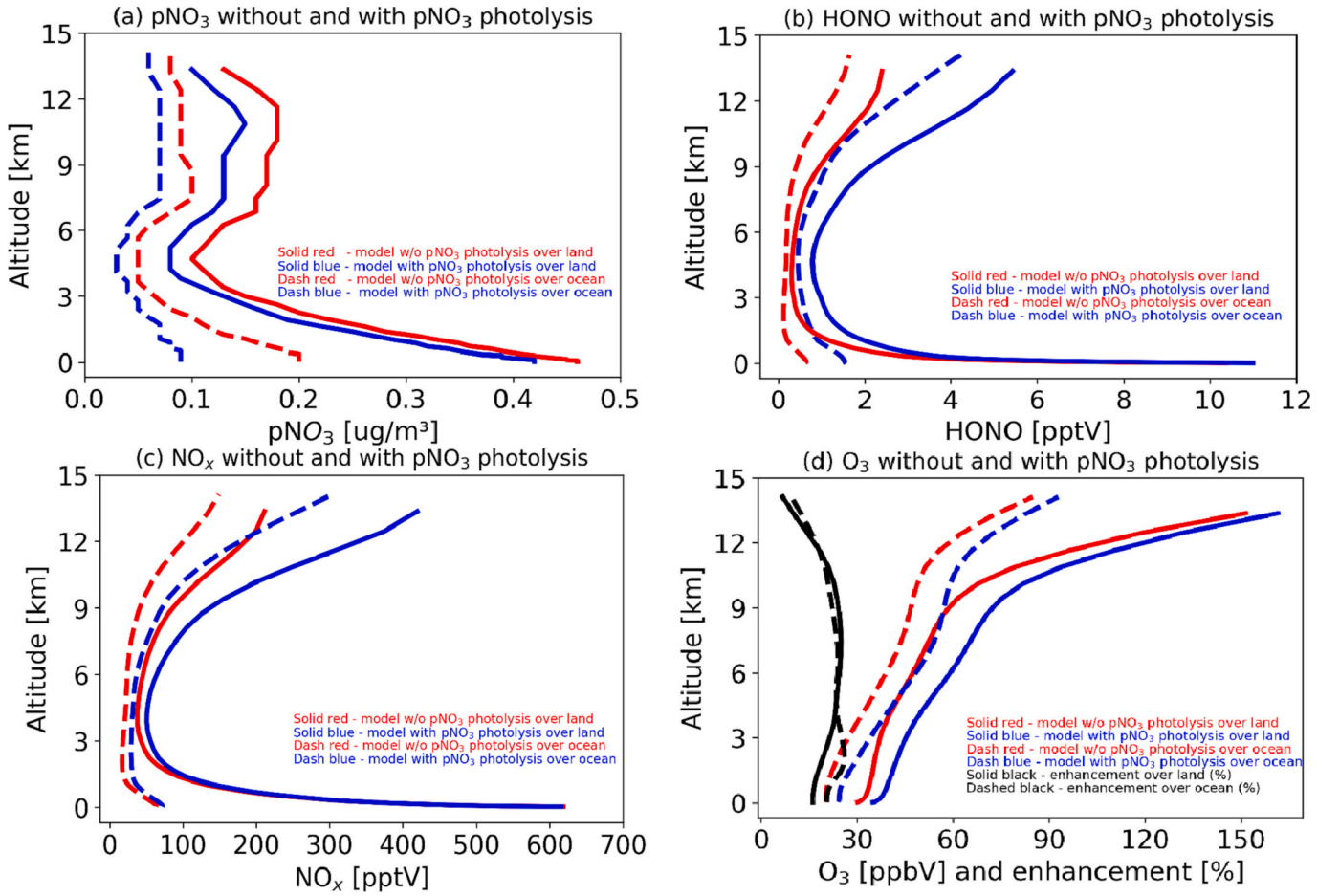

Fig. 2. Impact of pNO_3^- photolysis on (a) pNO_3^- concentrations, (b) HONO, (c) NO_x, and (d) O_3 mixing ratios at different altitudes.

photolysis and the changes in pNO_3^- due to the photolysis are shown in Fig. 3(a) and (b), respectively. Predicted surface pNO_3^- concentrations without the photolysis are higher over land and lower (generally <0.6 μg m^{-3}) over the ocean. Higher concentrations over China, India, western Europe, and eastern U.S. are noticeable. The chemistry reduces pNO_3^- over many ocean areas by 0.1–0.4 μg m^{-3}. In contrast, the impacts over land are smaller. pNO_3^- photolysis produces NO_2 and HONO which in turn undergoes photolysis producing OH. Enhanced OH then reacts with NO_2 to produce HNO_3 which partitions to pNO_3^-. Thus, the loss of pNO_3 due to photolysis is compensated for by the production of pNO_3^- from the $NO_2 + OH$ reaction. We compare model predictions with pNO_3^- measurements from the IMPROVE, the CASTNET, and the CSN. We calculate monthly Mean Bias (MB) using data over the entire U.S. and also only over the western U.S. (sites in California, Oregon, Washington, Idaho, Nevada, New Mexico, Wyoming, Colorado, Utah, Arizona, and Montana). As the impacts of the chemistry on pNO_3^- are small over the U.S. (Fig. 3(b)), the monthly MB without and with the chemistry do not change appreciably [Fig. 3(c) and (d)]. We also calculate monthly MB of

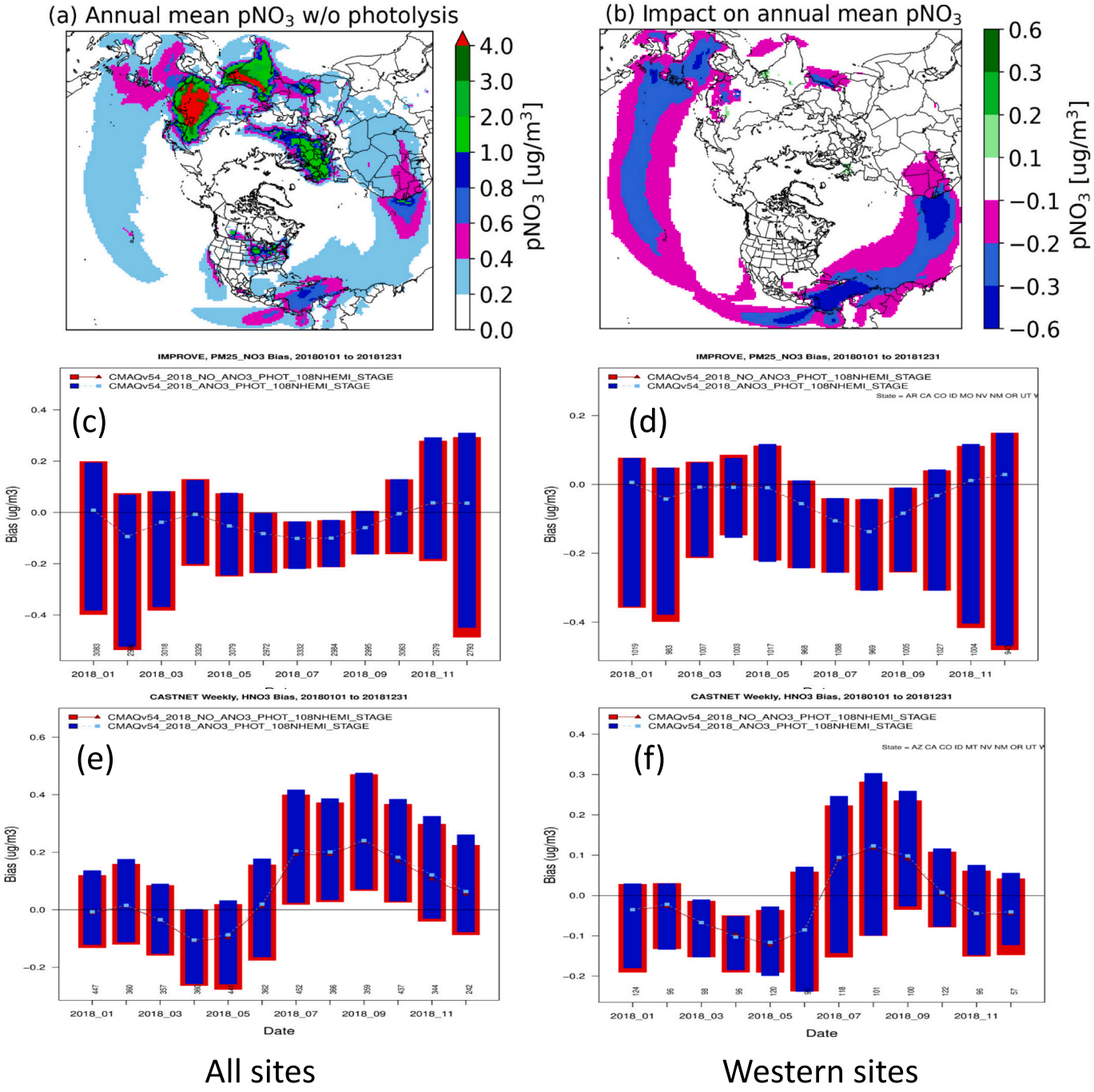

Fig. 3. (a) Annual mean daytime surface pNO_3^- concentrations without pNO_3^- photolysis; (b) changes in pNO_3^- concentrations with pNO_3^- photolysis compared to those without pNO_3^- photolysis; (c) monthly MB of pNO_3^- concentrations at the IMPROVE, CASTNET and CSN sites over the entire U.S.; and (d) monthly MB of pNO_3^- concentrations at the IMPROVE, CASTNET, and CSN sites over the western U.S. (e) monthly MB of HNO_3 mixing ratios at the CASTNET sites over the entire U.S.; and (f) monthly MB of HNO_3 mixing ratios at the CASTNET over the western U.S. For western U.S., all sites in California, Oregon, Washington, Idaho, Nevada, New Mexico, Wyoming, Colorado, Utah, Arizona, and Montana are used. Red color represents model without pNO_3^- photolysis and blue color represents model with pNO_3^- photolysis.

HNO_3 using model predictions and measurements from the CASTNET sites. The pNO_3^- photolysis does not affect the MB for the entire U.S. (Fig. 3(e)) or for predictions at the sites in the western U.S. (Fig. 3(f)).

Kelly et al. (2010) described sea-salt emissions in CMAQ and evaluated the model by comparing the model predictions to measurements from the Bay Regional Atmospheric Chemistry Experiment in Florida. Here, we show a comparison of model fine-mode sodium chloride (NaCl) concentrations to the measurements from the 13 coastal IMPROVE sites (Fig. S.1). Model tends to underestimate the observed data in most months in part due to coarse model grid resolution that may not adequately capture the magnitude of surf-zone sea-salt emissions. The underestimation of sea-salt concentrations also implies that model does not overestimate the enhancement factor (Eq. (2)).

3.3. Impact on annual daytime mean surface NO_2

Predicted annual daytime mean surface NO_2 without the photolysis and the changes in NO_2 due to the photolysis are shown in Fig. 4(a) and (b), respectively. Predicted surface NO_2 mixing ratios without the photolysis are higher over land and lower (generally <0.2 ppbV) over the ocean. Higher mixing ratios over China, India, western Europe, and eastern U.S. reflect higher NO_x (oxides of nitrogen) emissions over these areas. pNO_3^- photolysis directly produces NO_2 and enhances the levels over many ocean and land areas. It also decreases NO_2 over some areas due to enhanced reaction with OH.

We compare model predicted NO_2 vertical column density with the OMI satellite retrievals (Fig. 5). Seasonal MBs without the photolysis are generally negative over seawater as well as most continental land areas suggesting the model underpredicts NO_2 vertical column density compared to the satellite data. However, MBs with the photolysis are generally positive over much of the seawater and some land areas. The inclusion of pNO_3^- photolysis reduces the magnitude of the negative MBs over many land areas suggesting improvement of model predictions compared to satellite data. Greater improvements are seen in spring, summer, and fall, when photolysis frequencies are higher and lower improvements are seen in winter when photolysis frequencies are lower. CMAQ with pNO_3^- photolysis enhances annual NO_2 vertical column density by 28 % over the U.S. compared to the 13 % enhancement reported by Dang et al. (2023) using the GEOS-Chem model. It is difficult to exactly isolate the factors for such differences. Possible reasons include the differences in the treatment of emissions, vertical layer structures, and other items between the two models. We also compared model predictions with surface NO_2 measurements from the AQS sites across the U.S. AQS sites are generally located near urban areas where higher mixing ratios are present. Model changes near the surface are small; consequently, there are no changes in MBs (not shown) since the impacts near the surface are small.

3.4. Impact on annual daytime mean surface HONO

Predicted annual daytime mean surface HONO without the photolysis and the changes in HONO mixing ratios due to the photolysis are shown in Fig. 6(a) and (b), respectively. Predicted surface HONO mixing ratios without the photolysis are higher over land and lower (generally <1.0 pptV) over the ocean. CMAQ without pNO_3^- photolysis includes HONO emissions, gas-phase reactions, and heterogeneous reactions (Sarwar et al., 2008). Heterogeneous reactions of NO_2 on ground and aerosol surfaces are important for HONO production (Finlayson-Pitts and Pitts Jr., 2000; Aumont et al., 2003). Since NO_2 mixing ratios are higher over land, HONO mixing ratios are also generally higher over land. However, pNO_3^- photolysis enhances HONO over large areas of ocean and also over some areas of land, where NO_2 hydrolysis is a negligible source of HONO due to low NO_2 levels. We compare CMAQ predicted monthly mean diurnal HONO mixing ratios with the 2015 and 2023 measurements at CVAO (Fig. 6c). Both sets of measurements show higher daytime values than nighttime values. However, the 2023 daytime peak value is ~4 times greater than that in 2015. Andersen et al. (2023) reported measurements of HONO at CVAO in August 2019; their daytime peak is also larger than the 2015 data. Reasons for higher observed values in 2023 are not entirely clear. However, the measurements were completed in different years and months. It is plausible that HONO levels have increased during the measurement time period. We consider these two sets of data as the lower and upper bounds of measurements. We calculate monthly mean diurnal values using results from both model simulations and then also calculate annually aggregated diurnal mixing ratios using the monthly mean diurnal values (Fig. 6c). Predicted monthly mean diurnal HONO mixing ratios without pNO_3^- photolysis are substantially lower than the observed data and do not follow the variation in observed data. In contrast, monthly mean and annually aggregated diurnal HONO mixing ratios with pNO_3^- photolysis follow the variation in the observed data and most of the monthly mean and the annually aggregated diurnal mixing ratios fall within the upper and lower limits of the observed data. Zhang et al. (2022) recently reported HONO measurements at Beijing University, China in October 2018. Using the reported measured data, we calculate an average daytime value of 0.76 ppb (11–16 h) and nighttime value of 1.95 ppbv (remaining hours). In urban areas, HONO mixing ratios tend to be much higher than those in remote areas as shown in Fig. 6 and daytime observed HONO values are lower than corresponding nighttime values. In polluted urban atmosphere, NO_x reactions tend to be the main source for HONO formation. Model without pNO_3^- photolysis produces an average nighttime value of 0.91 ppbv and a daytime value of only 0.03 ppbv. Model predictions are lower than observed data due to two reasons: (1) this study uses a relatively coarse horizontal grid which artificially dilutes emitted NO_x over large grid volumes and subsequently produces lower HONO values (2) we previously implemented additional HONO reactions in CMAQ (Zhang et al., 2021) which improves the model comparison with observed HONO data in China. However, this

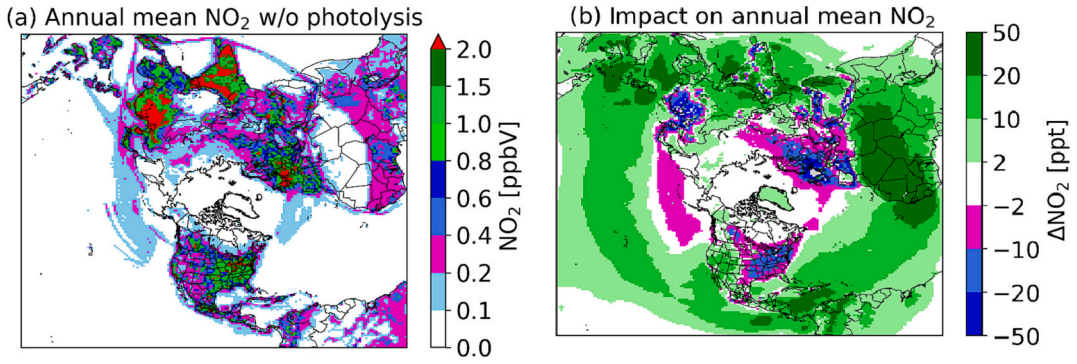

Fig. 4. (a) Annual mean surface NO_2 without pNO_3^- photolysis, and (b) changes in NO_2 with pNO_3 photolysis compared to those without pNO_3^- photolysis.

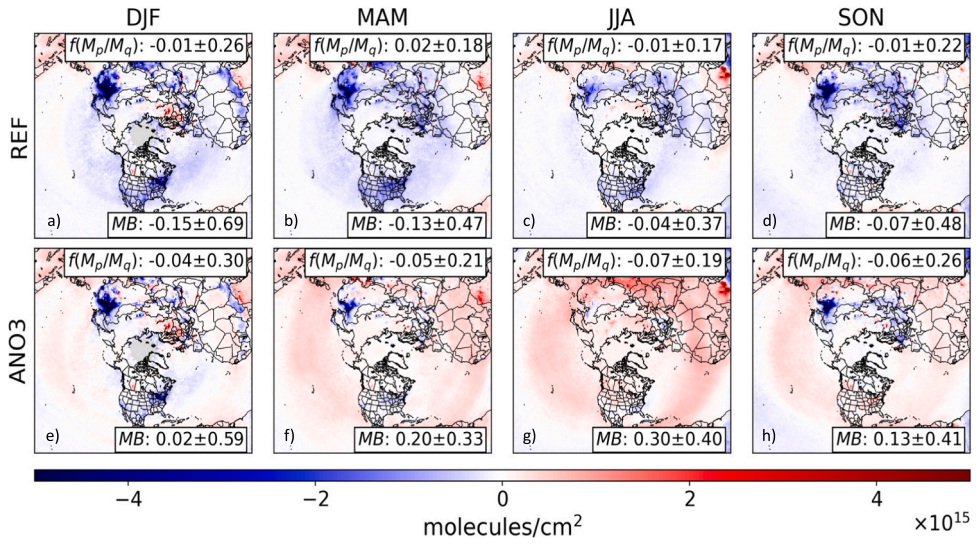

Fig. 5. Top panel: Seasonal MB of model NO_2 vertical column densities without pNO_3^- photolysis (calculated using satellite retrievals from the OMI): (a) winter (DJF) (b) spring (MAM) (c) summer (JJA) (d) fall (SON). Bottom panel: Seasonal MB of model NO_2 vertical column densities with pNO_3^- photolysis (calculated using satellite retrievals from the OMI): (e) winter (DJF) (f) spring (MAM) (g) summer (JJA) (h) fall (SON).

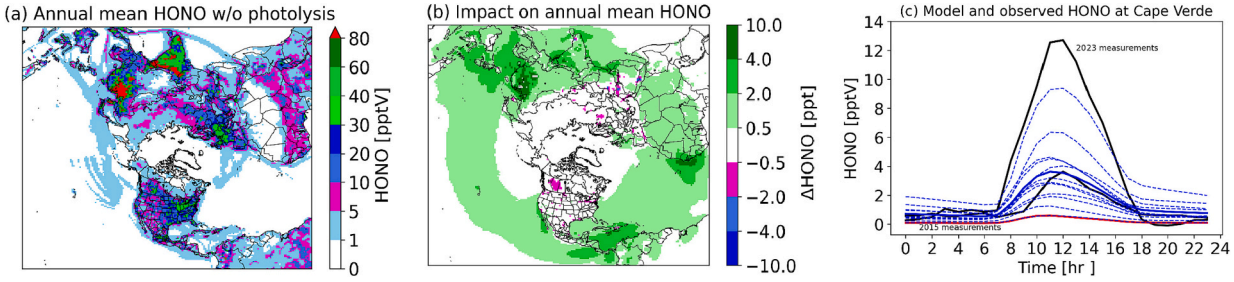

Fig. 6. (a) Annual daytime mean surface HONO without pNO_3^- photolysis; (b) changes in HONO mixing ratio with pNO_3^- photolysis compared to those without pNO_3^- photolysis; and (c) a comparison of model predicted diurnal HONO mixing ratios with measurements at the Cape Verde Atmospheric Observatory (CVAO): solid black colors represent measurements – upper black curve represents measurements in 2023 and lower black curve represents measurements in 2015; red solid curve represents the annual aggregate of monthly mean diurnal values from model without pNO_3^- photolysis; blue solid curve represents the annual aggregate of monthly mean diurnal values from model with pNO_3^- photolysis; blue dashed curves represent monthly mean diurnal values from model with pNO_3^- photolysis. Monthly mean diurnal mixing ratios from model without pNO_3^- photolysis are consistently lower than those with pNO_3^- photolysis and are not shown for clarity of the plot.

study did not consider those additional reactions. As expected, the model with pNO_3^- photolysis has small impact on HONO production in urban areas and produces similar HONO values (nighttime value = 0.92 ppbv and daytime value = 0.04 ppbv). Thus, the pNO_3^- photolysis does not appreciably alter the predicted HONO predictions in urban areas. Model predicts high levels of pNO_3^- over China, yields lower values of EF, and subsequently has low impacts on HONO. This reiterates that the chemistry is more important over remote areas where pNO_3^- can undergo photolysis at a higher frequency.

3.5. Impact on annual daytime mean surface OH

Predicted annual daytime mean surface OH mixing ratios without the photolysis and the absolute and relative changes due to the pNO_3^- photolysis are shown in Fig. 7(a)–(c), respectively. OH mixing ratios of <0.15 pptV are predicted over the remote marine atmosphere

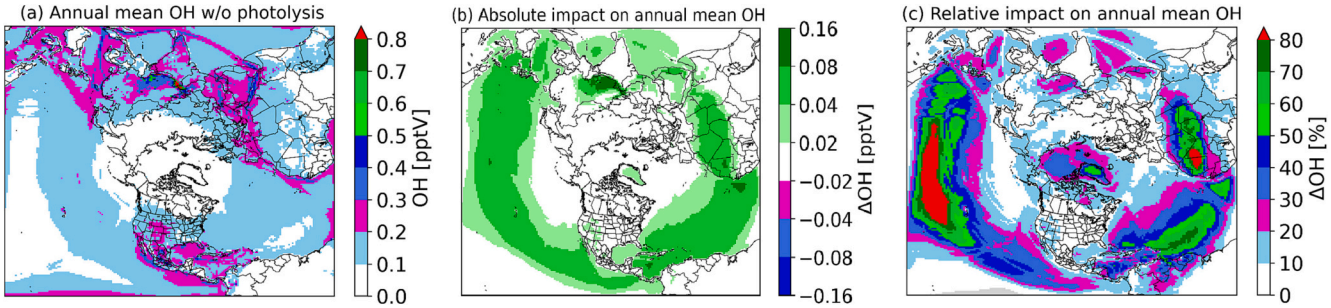

Fig. 7. (a) Annual mean daytime surface OH mixing ratio without pNO_3^- photolysis; (b) absolute changes in OH mixing ratio with pNO_3^- photolysis compared to those without pNO_3^- photolysis; and (c) relative changes in OH mixing ratios with pNO_3^- photolysis compared to those without pNO_3^- photolysis.

and higher mixing ratios (> ~ 0.2 pptV) are predicted over some land areas and along the shipping tracks where higher NO_x mixing ratios are predicted. pNO_3^- photolysis enhances OH substantially (0.04–0.08 pptV and > 50 %) over large areas of ocean and some areas of land. pNO_3^- photolysis directly enhances HONO which undergoes photolysis generating OH. Larger enhancements occur over marine environments than over land areas since more HONO and subsequently OH is produced over marine environments.

pNO_3^- photolysis in CMAQ enhances the maximum annual mean OH mixing ratio by a factor of ~2.0 compared to the Kasibhatla et al. (2018) reported largest impact of 1.6 over the marine boundary layer. CMAQ predicted impacts on OH are greater than the estimate of Kasibhatla et al. (2018) likely due to the fact that they used only coarse mode sea-salt pNO_3^- while we include all fine mode pNO_3^-. Kasibhatla et al. (2018) performed an additional simulation by adding the photolysis of accumulation-mode pNO_3^- and reported that it further enhanced OH by 4.6 % compared to that with the photolysis of coarse mode sea-salt pNO_3^-. Shah et al. (2023) reported a global OH mixing ratio increase of 19 % which agrees well with our estimated increase of 21 % over the Northern Hemisphere. Observed OH data are not publicly available for the simulation period. Whalley et al. (2010) reported the measurements of diurnal OH levels at the CVAO during May 29–June 2, 2007 using the Fluorescence Assay by Gas Expansion method. We qualitatively compare our model predictions with the reported measurements since the simulation and measurements are from different years. Measured mean peak occurred around noon and reached ~0.24 pptv. Model without pNO_3^- photolysis predicts a peak value of 0.34 pptv (average of May and June). Thus, model without pNO_3^- photolysis predicts 40 % higher value than the measurement. Measurements were completed in 2007 while the simulation was conducted for 2018. Similar to the HONO measurements, it is likely that OH levels at this location may have increased in recent years; consequently, model over-estimates the 2007 observed data. Model with pNO_3^- photolysis enhances peak OH level to 0.44 pptv; thus, the pNO_3^- photolysis enhances OH by 30 %.

3.6. Impact on annual and monthly daytime mean surface O_3

Predicted annual daytime mean surface O_3 without the photolysis and the changes due to the pNO_3^- photolysis are shown in Fig. 8(a) and (b), respectively. Predicted surface O_3 mixing ratios without pNO_3^- photolysis over land are greater than those over seawater. O_3 mixing ratios over seawater tend to be lower due to limited precursors and destruction by bromine (Fernandez et al., 2014) and iodine chemistry (Saiz-Lopez et al., 2014). Continental outflow regions have higher O_3 mixing ratios than over remote seawater. pNO_3^- photolysis enhances surface-level O_3 by 2–10 ppbv over large areas of the ocean as well as over land. The chemistry proceeds faster over seawater than over land, producing higher O_3 over seawater, which is subsequently transported over land. Areas of the Himalayas have larger impacts due to their higher elevation while areas of Africa have larger impacts due to wind-blown dust from the Sahara desert (see more in Section 4). Time series of monthly daytime mean surface O_3 mixing ratios over seawater and land without and with the chemistry are shown in Fig. 8(c). Predicted O_3 mixing ratios with the photolysis are consistently greater than those without the photolysis over seawater as well as land. Percent O_3 enhancements due to pNO_3^- photolysis over seawater and land are also shown in Fig. 8(c). Enhancements over seawater are consistently greater than those over land and the highest enhancement occurs in spring over both seawater and land.

Kasibhatla et al. (2018) reported O_3 enhancements of 1–5 ppbv over the marine boundary layer while Shah et al. (2023) reported a mean increase of 3.6 ppbv at the surface and a maximum increase of 8 ppbv. CMAQ predicts an increase in annual mean O_3 by 2–8 ppbv over the marine boundary layer, with a mean O_3 enhancement of 4.2 ppbv at the surface and a maximum increase of 14 ppbv. Thus, CMAQ predicted O_3 increases are larger than previous estimates reported by Kasibhatla et al. (2018) and Shah et al. (2023). The reasons for greater impacts in CMAQ are not clear. However, inherent model-to-model differences, and differences in horizontal grids and the representation and speciation of wind-blown dust likely contributed to larger enhancements.

We compare model predicted O_3 vertical column density with OMI satellite retrievals (Fig. 9a and b). MBs without pNO_3^- photolysis are generally negative over most of the seawater as well as continental land areas suggesting the model underpredicts O_3 vertical column density compared to the satellite data. However, MBs with the photolysis are positive over large areas suggesting the improvement of model predictions. Larger enhancements occur in the spring, summer, and fall season when photolysis is more active.

We compare model predicted O_3 mixing ratios with observed data from AQS and CASTNET sites in the U.S. and calculate monthly MBs without (red) and with (blue) the photolysis by using data over the entire U.S. as well as the western U.S. (Fig. 10a and b). For calculating MBs in the western U.S., we use data from all sites in California, Oregon, Washington, Idaho, Nevada, New Mexico, Wyoming, Colorado, Utah, Arizona, and Montana. Model performance without the photolysis is mixed – generally overpredicting observed O_3 in summer while underpredicting it in other seasons. pNO_3^- photolysis eliminates the negative bias for January–June both at CASTNET and AQS sites, improving the model performance. However, it increases MBs for the remaining months at both sites, deteriorating the model performance. When CASTNET and AQS sites only over the western U.S. are considered, MBs without the photolysis are negative for all months (except December at AQS sites) indicating that the model predictions are lower than the observed data. pNO_3^- photolysis eliminates the negative bias for all months (except January–March) at CASTNET sites and all months (except December) at AQS sites, leading to a substantial improvement of model performance. The existence of large springtime negative bias in CMAQ has been previously reported (Appel et al., 2021); pNO_3^- photolysis drastically rectifies the persistent negative bias in spring.

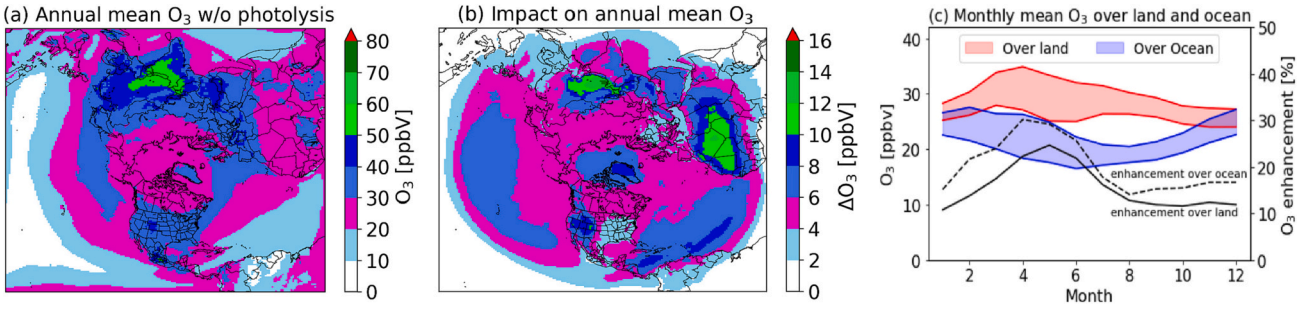

Fig. 8. (a) Annual daytime mean surface O_3 mixing ratios without pNO_3^- photolysis; (b) changes in O_3 mixing ratios with pNO_3^- photolysis compared to those without pNO_3^- photolysis; and (c) monthly mean surface O_3 mixing ratios without and with pNO_3^- photolysis over land and seawater and O_3 enhancements by the pNO_3^- photolysis over land and seawater.

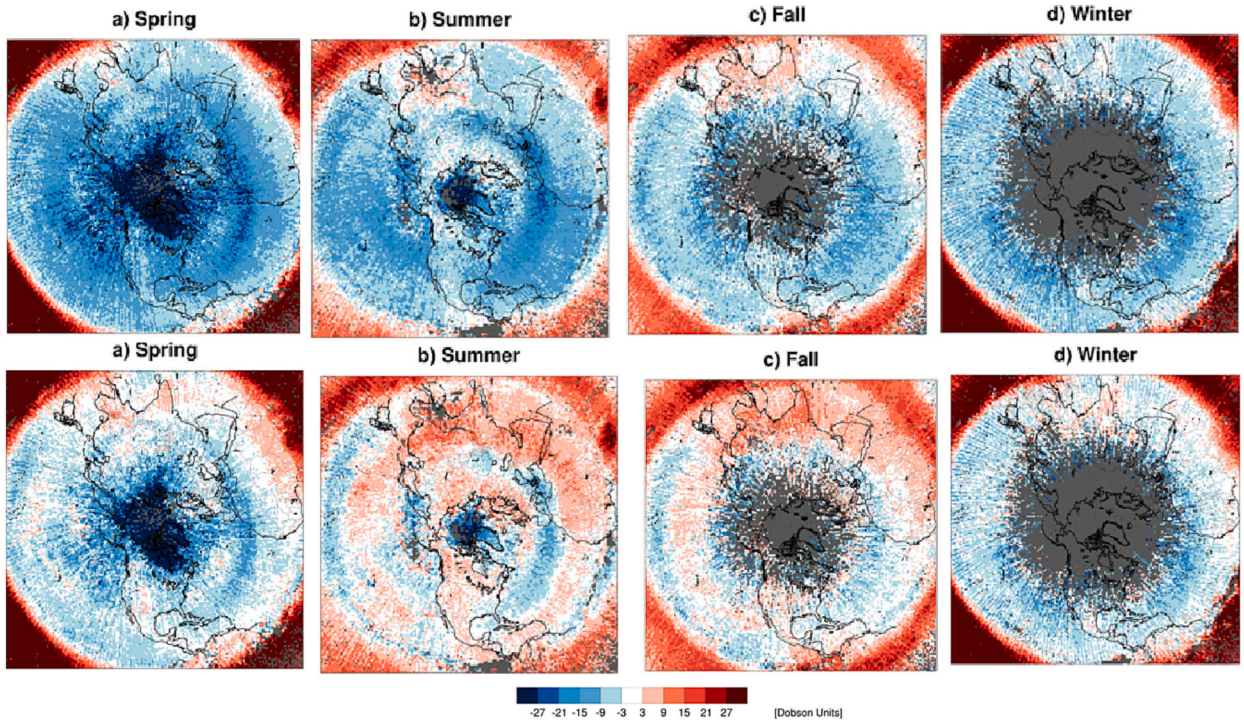

Fig. 9. Top panel: Seasonal MB of model O_3 vertical column densities without pNO_3^- photolysis (calculated using satellite retrievals from the OMI): (a) spring, (b) summer, (c) fall, (d) winter. Bottom panel: Seasonal MB of model O_3 vertical column densities with pNO_3^- photolysis (calculated using satellite retrievals from the OMI): (a) spring, (b) summer, (c) fall, (d) winter.

Thus, the pNO_3^- photolysis is particularly suitable for improving model O_3 concentrations during winter and spring, periods in which the model without the pNO_3^- photolysis exhibits systematic underestimation. However, during summer and fall the additional O_3 produced from this pathway degrades model performance at sites where the model without the pNO_3^- photolysis already overestimated the observed O_3.

MBs without and with pNO_3^- photolysis are also calculated using surface O_3 measurements from the NOAA ESRL sites (Fig. S.2(a)). The model without pNO_3^- photolysis consistently produces negative bias while the model with pNO_3^- photolysis improves the MBs for all months. We also calculate monthly MBs using data from the TOAR2 (Fig. S.2(b)) and over Japan (Fig. S.2(c)). Consistent with findings over the U.S., the model with pNO_3^- photolysis improves the comparison in cooler months and deteriorates the comparison in warmer months.

We show seasonal mean observed data from the OpenAQ sites over the Northern Hemisphere (Fig. S.3(a–d)). MBs without the photolysis are generally negative in spring (Fig. S.3(e)). In contrast, MBs without pNO_3^- photolysis are mixed in summer and fall - positive over some areas and negative over other areas (Fig. S.3(f–g)). The model performance is mixed in winter, over-predicting in some areas while under-predicting in other areas. The model with pNO_3^- photolysis consistently improves model performance in spring (Fig. S.3(i)), and has mixed impacts in other seasons (Fig. S.3(j–l)).

Comparison with ozonesonde measurements from the WOUDC and the NOAA ESRL are shown in Fig. 11. Data are separated by latitude and altitude. Model predictions without pNO_3^- photolysis are consistently lower than observed data at all altitudes and latitudes, revealing a large under-prediction of O_3 throughout the troposphere. In contrast, the model with pNO_3^- photolysis drastically improves the comparison with observed data, not only near the surface layers but also aloft, indicating a large improvement in model performance. At latitudes of $<45^0$ N, the model without the additional chemistry underestimates O_3 in several months during June and September (Fig. 11-b, d, f). However, model with the pNO_3^- photolysis tends to overestimate O_3 during this period likely due to the presence of high solar radiation which increases the photolysis frequency causing an overestimation of model O_3, suggesting possible seasonal variations in both the pNO_3^- photolysis frequency and the enhancement factor used in our parameterization. Nevertheless, the comparisons with ozonesonde measurements show that the inclusion of pNO_3^- photolysis helps rectify the systematic underestimation in springtime O_3 throughout the troposphere.

4. Sensitivity study

4.1. Impact of wind-blown dust on O_3 without and with pNO_3^- photolysis

Wind-blown dust in CMAQ produces pNO_3^- (Section 2) which can affect the impact of pNO_3^- photolysis on O_3. To isolate the impact associated with wind-blown dust on O_3, we performed two additional sensitivity simulations for January 2018. One simulation was conducted without wind-blown dust and using pNO_3^- photolysis. The other simulation was conducted without both wind-blown dust and pNO_3^- photolysis. Impacts of wind-blown dust on O_3 were calculated as the differences of mean O_3 with and without pNO_3^- photolysis (Fig. 12(a)–(c)). Wind-blown dust without pNO_3^- photolysis reduces O_3 over some areas of Asia by 1–2 ppbv since wind-blown dust attenuates sunlight, reducing photolysis frequencies and subsequently the O_3 formation rate. In contrast, wind-blown dust with pNO_3^- photolysis has a mixed impact on O_3 [Fig. 12(b)]. It reduces O_3 over parts of Asia and Africa but enhances O_3 over portions of Africa, South America, Asia, and the Atlantic Ocean. The inclusion of wind-blown dust with pNO_3^- photolysis can affect the chemistry in several ways. In CMAQ, wind-blown dust is speciated into several aerosol components, including pNO_3^-. The addition of wind-blown dust affects sunlight and reduces photolysis frequencies and O_3 formation rate. The additional pNO_3^- from wind-blown dust reduces EF (Eq. (2)), and also reduces pNO_3^- photolysis frequency and O_3 formation rate. However, the presence of additional pNO_3^- from wind-blown dust directly increases the availability of pNO_3^- and enhances the photolysis of pNO_3^- and O_3 formation rates. O_3 enhancement

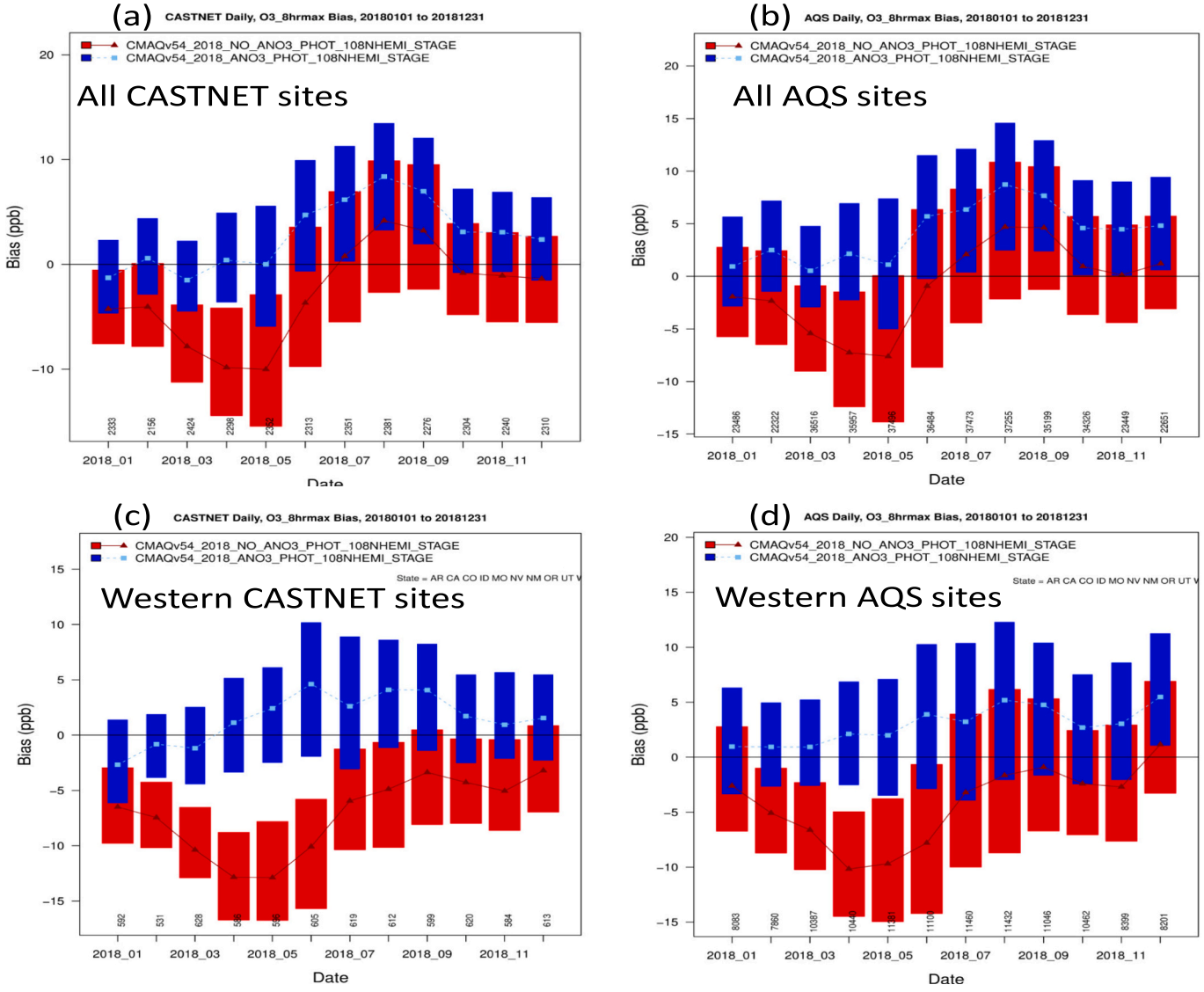

Fig. 10. (a) monthly MB of daily 8-hr maximum O_3 mixing ratios at the CASTNET sites calculated using data over the entire U.S.; (b) monthly MB of daily 8-hr maximum O_3 mixing ratios at AQS sites calculated using data over the entire U.S.; (c) monthly MB of daily 8-hr maximum O_3 mixing ratios at CASTNET sites calculated using data over the western U.S.; and (d) monthly MB of daily 8-hr maximum O_3 mixing ratios at AQS sites calculated using data over the western U.S. For western U.S., all sites in California, Oregon, Washington, Idaho, Nevada, New Mexico, Wyoming, Colorado, Utah, Arizona, and Montana are used. Red color indicates Bias without pNO_3^- photolysis and blue color indicates Bias with pNO_3^- photolysis. Red color represents model without pNO_3^- photolysis and blue color represents model with pNO_3^- photolysis.

rates outweigh the O_3 reduction rates over some areas, causing an increase in O_3 mixing ratios. The changes in wind-blown dust initiated O_3 [difference of Fig. 12(b) and (a)] are shown in Fig. 12(c). The enhancements of O_3 over the Sahara desert and surrounding areas are evident. Thus, wind-blown dust can have appreciable impact on pNO_3^- photolysis and affect O_3 mixing ratios in the vicinity of dust source areas. Using the GEOS-Chem model, Fairlie et al. (2010) reported that wind-blown dust can uptake HNO_3 and reduce surface O_3 mixing ratios over the North America by up to 1.0 ppbv. Koenig et al. (2021) recently performed aircraft measurements of iodine monoxide and other chemical species over the Atacama and Sechura Deserts and postulated that iodine released from dust can reduce O_3 over desert areas. However, CMAQ does not include HNO_3 uptake or release of iodine from dust; hence, the impact of such chemistry on O_3 is not accounted for in this study.

4.2. *Impact of NO_x reduction on O_3 without and with pNO_3^- photolysis*

To examine how pNO_3^- photolysis affects the relationship between O_3 abundance and NO_x emissions, we performed two additional sensitivity simulations for January 2018. One simulation was conducted without pNO_3^- photolysis and using 75 % of total NO_x emissions (25 % NO_x reduction). The other simulation was conducted with pNO_3^- photolysis and using 75 % of total NO_x emissions. The impact of lower NO_x emissions on O_3 was calculated as the difference of monthly mean O_3 with 75 % and 100 % NO_x emissions. The impacts of lower NO_x emissions on O_3 without pNO_3^- photolysis are shown in Fig. S.4(a). Lower NO_x emissions without pNO_3^- photolysis reduces O_3 over most areas of the modeling domain except over a portion of China, suggesting the area is a NO_x saturated region. The spatial impacts of lower NO_x emissions with pNO_3^- photolysis are also similar [Fig. S.4(b)]. The changes in O_3 due to lower NO_x emissions [difference of Fig. S.4(b) and (a)] are shown in Fig. S.4(c). The inclusion of pNO_3^- photolysis enhances the impact of NOx emission reductions on lowering O_3 concentrations

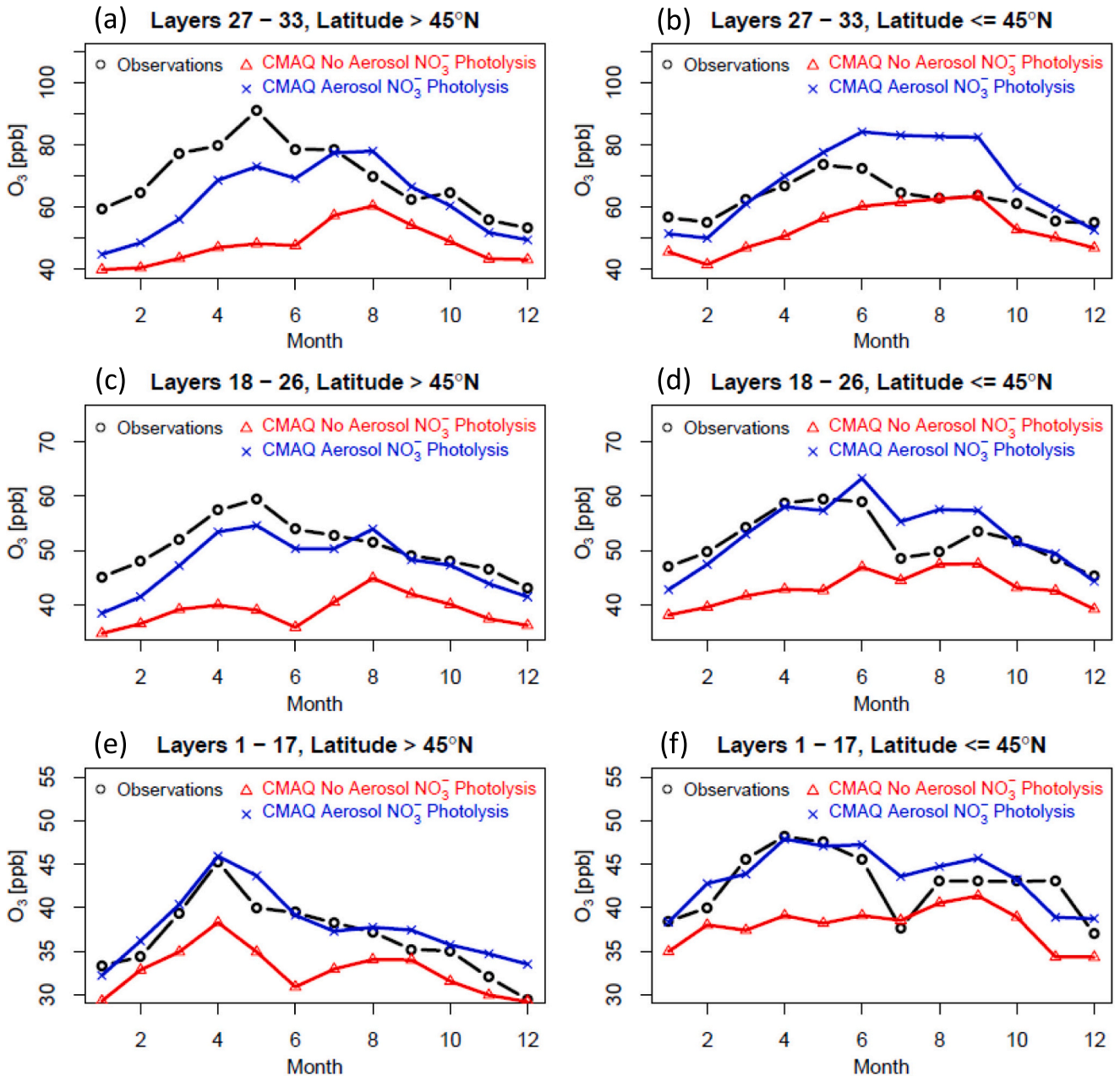

Fig. 11. A comparison of model O_3 mixing ratios with ozonesonde measurements from the WOUDC and the NOAA ESRL: (a) plot using data from 5.7 to 9.5 km at latitude $>45^0$ N; (b) plot using data from 5.7 to 9.5 km at latitude $<45^0$ N; (c) plot using data from 1.5 to 5.7 km at latitude $>45^0$ N; (d) plot using data from 1.5 to 5.7 km at latitude $<45^0$ N; (e) plot using data from 0 to 1.5 km at latitude $>45^0$ N; and (f) plot using data from 0 to 1.5 km at latitude $<45^0$ N. Black color represents observed data, red color represents model without pNO_3^- photolysis, and blue color represents model with pNO_3^- photolysis.

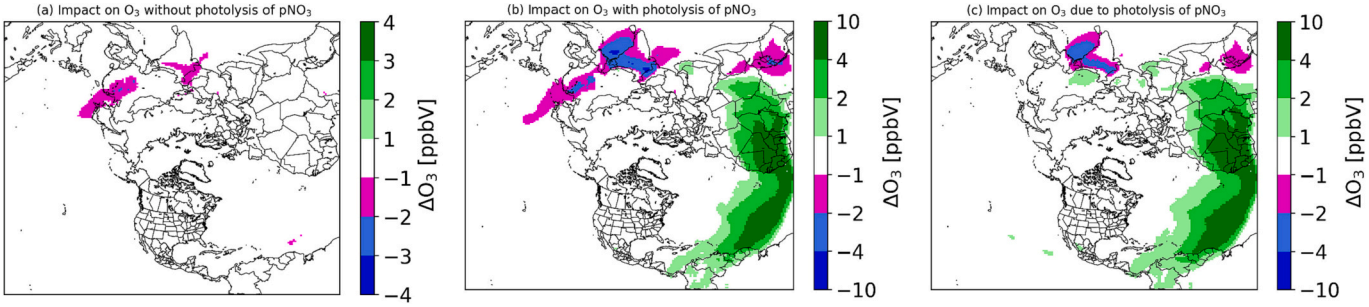

Fig. 12. (a) Impact of wind-blown dust on O_3 without pNO_3^- photolysis; (b) impact of wind-blown dust on O_3 with pNO_3^- photolysis; and (c) difference of the impact of wind-blown dust on O_3 with and without pNO_3^- photolysis

over portions of Africa, South America, India, and some oceanic areas by 0.3–3.0 ppbV O_3 for 25 % NO_x emission reduction. Thus, NO_x plays an important role in affecting O_3 through pNO_3^- photolysis. NO_x control is commonly employed for mitigating O_3 pollution. This result suggests that neglecting nitrate photolysis can lead to an underestimation in representing the potential benefit of NO_x reduction in lowering O_3. As seen in Fig. S4(c), greater reductions in O_3 are realized over marine areas influenced by continental transport of NO_x reservoir species highlighting the significance of this pathway in modulating large scale tropospheric O_3 distributions, especially as emissions across the globe change. The effects of pNO_3^- photolysis on modulating NO_x controls in coastal urban regions, however, cannot be robustly discerned using the coarse grid resolution employed by our current calculations and is an aspect that needs to be explored further with finer spatial resolution model calculations which can better resolve the interactions of this additional chemistry with that in urban plumes.

4.3. Impact of halogen chemistry on O_3 without and with pNO_3^- photolysis

To examine the impact of pNO_3^- photolysis on O_3 due to halogen (bromine and iodine) chemistry, we performed two additional sensitivity simulations for January 2018. One simulation was conducted without pNO_3^- photolysis and using no halogen chemistry and the other simulation was conducted with pNO_3^- photolysis and using no halogen chemistry. The impact of halogen chemistry on O_3 was calculated as the difference of monthly mean O_3 with and without halogen chemistry, without pNO_3^- photolysis and with pNO_3^- photolysis. Consistent with results of Sarwar et al. (2015) and Sarwar et al. (2019), halogen chemistry without pNO_3^- photolysis reduces O_3 not only over oceanic areas but also over land areas [Fig. S.5(a)]. However, the reductions over ocean areas are greater than those over land areas. The halogen chemistry with pNO_3^- photolysis also reduces O_3 over oceanic and land areas [Fig. S.5(b)]. However, the spatial impacts over the oceans are greater than those obtained without pNO_3^- photolysis; inclusion of photolysis further reduces O_3 over large oceanic areas by 0.5–3.0 ppbV [Fig. S.5(c)] due to two reasons. pNO_3^- photolysis increases O_3 which in turn enhances the iodine atom + O_3 and the bromine atom + O_3 reaction rates causing an additional O_3 loss. CMAQ uses the MacDonald et al. (2014) parameterization for estimating inorganic iodine emissions due to the interaction of iodide in seawater and O_3. Enhanced O_3 due to pNO_3^- photolysis increases inorganic iodine emissions which enhance the iodine atom + O_3 reaction rates causing a further O_3 loss.

4.4. Impact of DMS chemistry modulated O_3 without and with pNO_3^- photolysis

To examine the impact of pNO_3^- photolysis on O_3 due to DMS (dimethyl sulfide) chemistry, we performed two additional sensitivity simulations for January 2018. One simulation was conducted without pNO_3^- photolysis and without any DMS chemistry (note that inclusion of DMS chemistry is default in the cb6r5m chemical mechanism). The other simulation was conducted with pNO_3^- photolysis and without any DMS chemistry. We calculated the DMS chemistry modulated impact on O_3 as the difference of monthly mean O_3 with and without DMS chemistry. As expected, the DMS chemistry modulated impact on O_3 without pNO_3^- photolysis is small ($< \pm 1.0$ ppbV) [Fig. S.6(a)]. However, the DMS chemistry modulated impacts on O_3 with pNO_3^- photolysis are greater than those without pNO_3^- photolysis as the process reduces O_3 over large oceanic and land areas by 1.0–6.0 ppbV [Fig. S.6 (b)]. DMS chemistry not only enhances sulfate but also reduces pNO_3^- over oceanic areas (Zhao et al., 2021; Sarwar et al., 2023). The model with pNO_3^- photolysis and DMS chemistry reduces more O_3 since pNO_3^- concentrations are lower compared to the levels without DMS chemistry. The changes in DMS modulated O_3 [difference of Fig. S.6(b) and (a)] are shown in Fig. S.6(c).

5. Summary

We implemented pNO_3^- photolysis into CMAQv5.4 by adopting the parametrization of Shah et al. (2023) for calculating the pNO_3^- photolysis frequency of fine mode pNO_3^- and perform annual simulations without and with pNO_3^- photolysis and examine its impacts on air quality over the Northern Hemisphere. Model results suggest that the chemistry reduces pNO_3^- concentrations and enhances NO_2, HONO, and OH mixing ratios, mostly over seawater. Additionally, the incorporation of this pathway increases O_3 over seawater as well as land, with peak enhancements occurring in spring. Enhanced O_3 mixing ratios compare better with available surface measurements over the U.S., Japan, and TOAR2, and improve the model performance, in particular substantially improving the springtime low bias in CMAQ. The enhancement in modeled O_3 occurs not only at the surface but also aloft and results in improved comparisons with three-dimensional O_3 distributions represented with available ozonesonde observations. The improvements in aloft O_3 distributions result in better characterization of long-range transported O_3 in the troposphere (as evident by comparisons with ozonesonde data) and its subsequent modulation of surface O_3 in downwind continental regions as also demonstrated by improved comparison of spring-time surface O_3 predictions with ground-based measurements. We find that the pNO_3^- photolysis pathway has large impacts on model results, highlighting the need for additional field and experimental studies to better constrain pNO_3^- photolysis frequencies and reduce the uncertainty in its estimated impacts on modulating tropospheric composition and air quality across the globe.

Disclaimer

The views expressed in this paper are those of the authors and do not necessarily represent the views or policies of the U.S. EPA. Mention of trade names or commercial products does not constitute endorsement or recommendation for use.

CRediT authorship contribution statement

Golam Sarwar: Writing – original draft, Investigation, Conceptualization. **Christian Hogrefe:** Writing – review & editing, Investigation. **Barron H. Henderson:** Writing – review & editing, Investigation. **Rohit Mathur:** Writing – review & editing, Investigation. **Robert Gilliam:** Investigation, Writing – review & editing. **Anna B. Callaghan:** Writing – review & editing, Data curation. **James Lee:** Writing – review & editing, Data curation. **Lucy J. Carpenter:** Writing – review & editing, Data curation.

Declaration of competing interest

The authors declare that they have no known competing financial interests or personal relationships that could have appeared to influence the work reported in this paper.

Data availability

CMAQ source code is publicly available from the following website: https://github.com/USEPA/CMAQ.

Acknowledgements

We thank Viral Shah at the National Aeronautics and Space Administration (NASA) Goddard Space Flight Center for highlighting the importance of this chemistry and for useful conversations about the interactions within the modeling systems. We also thank the maintainers

of the AQS, CASTNET, IMPROVE, TOAR2, OpenAQ, and NOAA ESRL data portals from which the surface ozone observations used in this study were obtained. We would also like to acknowledge NOAA ESRL and the World Ozone and UV Data Center for making the ozonesonde measurements available and the NASA for availability of remote sensing retrievals from the OMI. The HONO and supporting measurements at the CVAO were supported by funding from the UK Natural Environment Research Council (NERC).

Appendix A. Supplementary data

Supplementary data to this article can be found online at https://doi.org/10.1016/j.scitotenv.2024.170406.

References

Andersen, S.T., Carpenter, L.J., Reed, C., Lee, J.D., Chance, R., Sherwen, T., Vaughan, A. R., Stewart, J., Edwards, P.M., Bloss, W.J., Sommariva, R., Crilley, L.R., Nott, G.J., Neves, L., Read, K., Heard, D.E., Seakins, P.W., Whalley, L.K., Boustead, G.A., Fleming, L.T., Stone, D., Fomba, K.W., 2023. Extensive field evidence for the release of HONO from the photolysis of nitrate aerosols. Sci. Adv. 9(3):eadd6266 https://doi.org/10.1126/sciadv.add6266.

Appel, K.W., et al., 2021. The community multiscale air quality (CMAQ) model versions 5.3 and 5.3.1: system updates and evaluation. Geosci. Model Dev. 14, 2867–2897. https://doi.org/10.5194/gmd-14-2867-2021.

Atkinson, R., Baulch, D.L., Cox, R.A., Crowley, J.N., Hampson, R.F., Hynes, R.G., Jenkin, M.E., Rossi, M.J., Troe, J., 2004. Evaluated kinetic and photochemical data for atmospheric chemistry: volume I - gas phase reactions of O_x, HO_x, NO_x and SO_x species. Atmos. Chem. Phys. 4, 1461–1738. https://doi.org/10.5194/acp-4-1461-2004.

Aumont, B., Chervier, F., Laval, S., 2003. Contribution of HONO sources to the NO_x/HO_x/O_3 chemistry in the polluted boundary layer. Atmos. Environ. 37, 487–498.

Bao, F., Li, M., Zhang, Y., Chen, C., Zhao, J., 2018. Photochemical aging of Beijing urban PM2.5: HONO production. Env. Sci. Tech. 52 (11), 6309–6316.

Binkowski, F.S., Roselle, S.J., 2003. Community Multiscale Air Quality (CMAQ) model aerosol component, I: Model description. J. Geophys. Res. 108, 4183. https://doi.org/10.1029/2001JD001409.

Cao, Y., Ma, Q., Chu, B., He, H., 2023. 2023: homogeneous and heterogeneous photolysis of nitrate in the atmosphere: state of the science, current research needs, and future prospects. Front. Environ. Sci. Eng. 17 (4), 48.

Dang, R., Jacob, D.J., Shah, V., Eastham, S.D., Fritz, T.M., Mickley, L.J., Liu, T., Wang, Y., Wang, J., 2023. Background nitrogen dioxide (NO_2) over the United States and its implications for satellite observations and trends: effects of nitrate photolysis, aircraft, and open fires. Atmos. Chem. Phys. 23, 6271–6284. https://doi.org/10.5194/acp-23-6271-2023.

Fairlie, T.D., Jacob, D.J., Dibb, J.E., Alexander, B., Avery, M.A., van Donkelaar, A., Zhang, L., 2010. Impact of mineral dust on nitrate, sulfate, and ozone in transpacific Asian pollution plumes. Atmos. Chem. Phys. 10, 3999–4012. https://doi.org/10.5194/acp-10-3999-2010.

Fernandez, R.P., Salawitch, R.J., Kinnison, D.E., Lamarque, J.-F., Saiz-Lopez, A., 2014. Bromine partitioning in the tropical tropopause layer: implications for stratospheric injection. Atmospheric Chemistry and Physics 14, 13391–13410.

Finlayson-Pitts, B.J., Pitts Jr., J.N., 2000. Chemistry of the Upper Lower Atmosphere. Experiments and Applications, Academic Press, San Diego, Theory.

Foley, K.M., Pouliot, G.A., Eyth, A., Aldridge, M.F., Allen, C., Appel, K.W., Bash, J.O., Beardsley, M., Beidler, J., Choi, D., Farkas, C., Gilliam, R.C., Godfrey, J., Henderson, B.H., Hogrefe, C., Koplitz, S.N., Mason, R., Mathur, R., Misenis, C., Possiel, N., Pye, H.O.T., Reynolds, L., Roark, M., Roberts, S., Schwede, D.B., Seltzer, K.M., Sonntag, D., Talgo, K., Toro, C., Vukovich, J., Xing, J., Adams, E., 2023. 2002-2017 anthropogenic emissions data for air quality modeling over the United States. Data Brief 47, 109022. https://doi.org/10.1016/j.dib.2023.109022.

Fountoukis, C. and Nenes, A., 2007: ISORROPIA II: a computationally efficient thermodynamic equilibrium model for K^+-Ca^{2+}-Mg^{2+}-NH_4^+-SO_4^{2-}-NO_3^--Cl-H_2O aerosols, Atmos. Chem. Phys., 7, 4639–4659.

Fu, X., Wang, T., Zhang, L., Li, Q., Wang, Z., Xia, M., Yun, H., Wang, W., Yu, C., Yue, D., Zhou, Y., Zheng, J., Han, R., 2019. The significant contribution of HONO to secondary pollutants during a severe winter pollution event in southern China. Atmos. Chem. Phys. 19, 1–14.

Gantt, B., Kelly, J.T., Bash, J.O., 2015. Updating Sea spray aerosol emissions in the community multiscale air quality (CMAQ) model version 5.0.2. Geoscientific Model Development Discussions 8, 3905–3939.

Gen, M., Liang, Z., Zhang, R., Mabato, B., R, G,; Chan, C. K., 2022. Particulate nitrate photolysis in the atmosphere. Environmental Science: Atmospheres 2 (2), 111–127.

Gilliam, R.C., Foley, K., Reynolds, L., Bash, J., Hogrefe, C., Mathur, R., Possiel, N., Misenis, C., Henderson, B., Sarwar, G., Appel W., and Pouliot G., 2021. An evaluation of a two-decade CONUS and Northern Hemispheric timeseries of retrospective WRF simulations. 20th Annual CMAS Conference, November 1–4, 2021, Chapel Hill, NC. Available at: https://www.cmascenter.org/conference/2021/slides/gilliam-retrospective-wrf-simulations-2021.pdf.

Heland, J., Kleffmann, J., Kurtenbach, R., Wiesen, P., 2001. A new instrument to measure gaseous nitrous acid (HONO) in the atmosphere. Environ. Sci. Technol. 35, 3207–3212. https://doi.org/10.1021/es000303t.

Hoesly, R.M., Smith, S.J., Feng, L., Klimont, Z., Janssens-Maenhout, G., Pitkanen, T., Seibert, J.J., Vu, L., Andres, R.J., Bolt, R.M., Bond, T.C., Dawidowski, L., Kholod, N., Kurokawa, J.-I., Li, M., Liu, L., Lu, Z., Moura, M.C.P., O'Rourke, P.R., Zhang, Q., 2018. Historical (1750–2014) anthropogenic emissions of reactive gases and aerosols from the community emissions data system (CEDS). Geosci. Model Dev. 11, 369–408. https://doi.org/10.5194/gmd-11-369-2018.

Janssens-Maenhout, G., Crippa, M., Guizzardi, D., Dentener, F., Muntean, M., Pouliot, G., Keating, T., Zhang, Q., Kurokawa, J., Wankmüller, R., Denier van der Gon, H., Kuenen, J.J.P., Klimont, Z., Frost, G., Darras, S., Koffi, B., Li, M., 2015. HTAP_v2.2, 2015: a mosaic of regional and global emission grid maps for 2008 and 2010 to study hemispheric transport of air pollution. Atmos. Chem. Phys. 15, 11411–11432. https://doi.org/10.5194/acp-15-11411-2015.

Kang, D., Willison, J., Sarwar, G., Madden, M., Hogrefe, C., Mathur, R., Gantt, B., Saiz-Lopez, A., 2021. Improving the characterization of natural emissions in CMAQ. EM Magazine, Air and Waste Management Association, Pittsburgh, PA 10, 1–7.

Kasibhatla, P., Sherwen, T., Evans, M.J., Carpenter, L.J., Reed, C., Alexander, B., Chen, Q., Sulprizio, M.P., Lee, J.D., Read, K.A., Bloss, W., Crilley, L.R., Keene, W.C., Pszenny, A.A.P., Hodzic, A., 2018. Global impact of nitrate photolysis in sea-salt aerosol on NO_x, OH, and O_3 in the marine boundary layer. Atmos. Chem. Phys. 18, 11185–11203. https://doi.org/10.5194/acp-18-11185-2018.

Kelly, J.T., Bhave, P.V., Nolte, C.G., Shankar, U., Foley, K.M., 2010. 2010: simulating emission and chemical evolution of coarse sea-salt particles in the community multiscale air quality (CMAQ) model. Geosci. Model Dev. 3, 257–273. https://doi.org/10.5194/gmd-3-257-2010.

Kitayama, K., Morino, Y., Yamaji, K., Chatani, S., 2019. Uncertainties in O_3 concentrations simulated by CMAQ over Japan using four chemical mechanisms. Atmos. Environ. 198 (1), 448–462.

Kleffmann, J., Heland, J., Kurtenbach, R., Lorzer, J., Wiesen, P., 2002. A new instrument (LOPAP) for the detection of nitrous acid (HONO). Environ. Sci. Pollut. R. 1, 48–54.

Koenig, T.K., Volkamer, R., Apel, E.C., Bresch, J.F., Cuevas, C.A., Dix, B., Eloranta, E.W., Fernandez, R.P., R. Hall, S.R., Hornbrook, R.S., Pierce, R.B., Reeves, J.M., Saiz-Lopez, A., Ullmann, K., 2021. Ozone depletion due to dust release of iodine in the free troposphere. Sci. Adv. 7, eabj6544.

MacDonald, S.M., Martin, J.C.G., Chance, R., Warriner, S., Saiz-Lopez, A., Carpenter, L. J., Plane, J.M.C., 2014. A laboratory characterisation of inorganic iodine emissions from the sea surface: dependence on oceanic variables and parameterisation for global modelling. Atmospheric Chemistry & Physics 14, 5841–5852.

Mathur, R., Xing, J., Gilliam, R., Sarwar, G., Hogrefe, C., Pleim, J., et al., 2017. Extending the Community Multiscale Air Quality (CMAQ) modeling system to hemispheric scales: overview of process considerations and initial applications. Atmos. Chem. Phys. 17 (20), 12449–12474. https://doi.org/10.5194/acp-17-12449-2017.

Mathur, R., Kang, D., Sergey Napelenok, S., Xing, J., Hogrefe, C., Sarwar, G., Syuichi Itahashi, S., Henderson, B., 2022. How are divergent global emission trends influencing long-range transported ozone to North America? J. of Geophysical Research–Atmospheres 127 (16).

Millero, F.J., 1996. Chemical Oceanography, second ed. CRC Press, Boca Raton, FL.

Murphy, B.N., Woody, M.C., Jimenez, J.L., Carlton, A.M.G., Hayes, P.L., Liu, S., Ng, N.L., Russell, L.M., Setyan, A., Xu, L., Young, J., Zaveri, R.A., Zhang, Q., Pye, H.O.T., 2017. Semivolatile POA and parameterized total combustion SOA in CMAQv5.2: impacts on source strength and partitioning. Atmospheric Chemistry & Physics 17, 11107–11133. https://doi.org/10.5194/acp-17-11107-2017.

Price, C.G., Penner, J.E., Prather, M.J., 1997. NOx from lightning, part I: global distribution based on lightning physics. J. Geophys. Res. 102, 5229–5241.

Reed, et al., 2017. Evidence for renoxification in the tropical marine boundary layer. Atmos. Chem. Phys. 17, 4081–4092.

Romer, P.S., Wooldridge, P.J., Crounse, J.D., Kim, M.J., Wennberg, P.O., Dibb, J.E., Scheuer, E., Blake, D.R., Meinardi, S., Brosius, A.L., Thames, A.B., Miller, D.O., Brune, W.H., Hall, S.R., Ryerson, T.B., Cohen, R.C., 2018. Constraints on aerosol nitrate photolysis as a potential source of HONO and NO_x. Environ Sci Technology 52 (23), 13738–13746. https://doi.org/10.1021/acs.est.8b03861.

Saiz-Lopez, A., Fernandez, R.P., Ordóñez, C., Kinnison, D.E., Gómez Martín, J.C., Lamarque, J.-F., Tilmes, S., 2014. Iodine chemistry in the troposphere and its effect on ozone. Atmos. Chem. Phys. 14, 13119–13143.

Sarwar, G., Roselle, S.J., Mathur, R., Appel, W., Dennis, R.L., Vogel, B., 2008. A comparison of CMAQ HONO predictions with observations from the northeast oxidant and particle study. Atmos. Environ. 42, 5760–5770.

Sarwar, G., Simon, H., Bhave, P., Yarwood, G., 2012. Examining the impact of heterogeneous nitryl chloride production on air quality across the United States. Atmospheric Chemistry & Physics 12, 1–19.

Sarwar, G., Gantt, B.; Schwede, D.; Foley, K.; Mathur, R.; Saiz-Lopez, A., 2015. Impact of enhanced ozone deposition and halogen chemistry on tropospheric ozone over the northern hemisphere, Environ. Sci. Technol., 2015, 49(15):9203–9211.

Sarwar, G., Gantt, B., Foley, K., Fahey, K., Spero, T.L., Kang, D., Mathur, Rohit M., Hosein, F., Xing, J., Sherwen, T., Saiz-Lopez, A., 2019. Influence of bromine and iodine chemistry on annual, seasonal, diurnal, and background ozone: CMAQ simulations over the northern hemisphere. Atmos. Environ. 213, 395–404.

Sarwar, G., Kang, D., Henderson, B.H., Hogrefe, C., Appel, W., Mathur, R., 2023. Examining the impact of dimethyl sulfide emissions on atmospheric sulfate over the continental U.S. Atmosphere 14, 660. https://doi.org/10.3390/atmos14040660.

Shah, V., Jacob, D.J., Dang, R., Lamsal, L.N., Strode, S.A., Steenrod, S.D., Boersma, K.F., Eastham, S.D., Fritz, T.M., Thompson, C., Peischl, J., Bourgeois, I., Pollack, I.B., Nault, B.A., Cohen, R.C., Campuzano-Jost, P., Jimenez, J.L., Andersen, S.T., Carpenter, L.J., Sherwen, T., Evans, M.J., 2023. Nitrogen oxides in the free

troposphere: implications for tropospheric oxidants and the interpretation of satellite NO_2 measurements. Atmos. Chem. Phys. 23, 1227–1257. https://doi.org/10.5194/acp-23-1227-2023.

Sherwen, T., Schmidt, J.A., Evans, M.J., Carpenter, L.J., Großmann, K., Eastham, S.D., Jacob, D.J., Dix, B., Koenig, T.K., Sinreich, R., Ortega, I., Volkamer, R., Saiz-Lopez, A., Prados-Roman, C., Mahajan, A.S., Ordóñez, C., 2016. Global impacts of tropospheric halogens (cl, Br, I) on oxidants and composition in GEOS-Chem. Atmos. Chem. Phys. 16, 12239–12271.

Shi, Q., Tao, Y., Krechmer, J.E., Heald, C.L., Murphy, J.G., Kroll, J.H., Ye, Q., 2021. Laboratory investigation of Renoxification from the photolysis of inorganic particulate nitrate. Environ. Sci. Technol. 55 (2), 854–861. https://doi.org/10.1021/acs.est.0c06049.

Simon, H., Beck, L., Bhave, P.V., Divita, F., Hsu, Y., Luecken, D., Mobley, J.D., Pouliot, G. A., Reff, A., Sarwar, G., Strum, M., 2010. The development and uses of EPA's SPECIATE database. Atmos. Pollut. Res. 1, 196–206.

Sindelarova, K., Granier, C., Bouarar, I., Guenther, A., Tilmes, S., Stavrakou, T., Müller, J. F., Kuhn, U., Stefani, P., Knorr, W., 2014. Global data set of biogenic VOC emissions calculated by the MEGAN model over the last 30 years. Atmos. Chem. Phys. 14, 9317–9341. https://doi.org/10.5194/acp-14-9317-2014.

Skamarock, W.C., 2008. A description of the advanced research WRF version 3. NCAR Tech Note NCAR/TN 475 STR, 125 pp. [Available from UCAR Communications, P.O. Box 3000, Boulder, CO 80307.].

Whalley, L.K., Furneaux, K.L., Goddard, A., Lee, J.D., Mahajan, A., Oetjen, H., Read, K.A., Kaaden, N., Carpenter, L.J., Lewis, A.C., Plane, J.M.C., Saltzman, E.S., Wiedensohler, A., Heard, D.E., 2010. The chemistry of OH and HO_2 radicals in the boundary layer over the tropical Atlantic Ocean. Atmos. Chem. Phys. 10, 1555–1576. https://doi.org/10.5194/acp-10-1555-2010.

Wiedinmyer, C., Akagi, S. K., Yokelson, R. J., Emmons, L. K., Al-Saadi, J. A., Orlando, J. J., and Soja, A.J The Fire INventory from NCAR (FINN), 2011:a high resolution global model to estimate the emissions from open burning, Geosci. Model Dev., 4, 625–641, https://doi.org/10.5194/gmd-4-625-2011 2011.

Yarwood, G., Shi, Y., Beardsley, R., 2020. Impact of CB6r5 Mechanism Changes on Air Pollutant Modeling in Texas, Final Report to Texas Commission on Environmental Quality, Work Order No. 582–20–11221-014, July, 2020.

Ye, C., Zhou, X., Pu, D., et al., 2016. Rapid cycling of reactive nitrogen in the marine boundary layer. Nature 532, 489–491. https://doi.org/10.1038/nature17195.

Ye, C., Zhang, Ni, Gao, H., Zhou, X., 2017. Photolysis of particulate nitrate as a source of HONO and NO_x. Environ. Sci. Technol. 51 (12), 6849–6856. https://doi.org/10.1021/acs.est.7b00387.

Ye, C., Zhou, X., Pu, D., Stutz, J., Festa, J., Spolaor, M., Tsai, C., Cantrell, C., Mauldin III, R.L., Weinheimer, A., Hornbrook, R.S., Apel, E.C., Guenther, A., Kaser, L., Yuan, B., Karl, T., Haggerty, J., Hall, S., Ullmann, K., Smith, J., Ortega, J., 2018. Tropospheric HONO distribution and chemistry in the southeastern US. Atmos. Chem. Phys. 18, 9107–9120. https://doi.org/10.5194/acp-18-9107-2018.

Zhang, J., Chaofan, L., Weigang, W., Ge, M., Guo, Y., Ran, H., Zhang, Y., Zheng, F., Fan, X., Yan, C., Daellenbach, K.R., Liu, Y., Kulmala, M., An, J., 2022. Amplified role of potential HONO sources in O_3 formation in North China plain during autumn haze aggravating processes. Atmos. Chem. Phys. 22, 3275–3302.

Zhang, S., Sarwar, G., Xing, J., Chu, B., Xue, C., Sarav, A., Ding, D., Zheng, H., Mu, Y., Duan, F., Ma, T., He, H., 2021. Improving the representation of HONO chemistry in CMAQ and examining its impact on haze over China. Atmos. Chem. Phys. 21, 15809–15826.

Zhao, J., Sarwar, G., Gantt, B., Foley, K., Henderson, B.H., Pye, H.O.T., Fahey, K.M., Kang, D., Mathur, R., Zhang, Y., Li, Q., Saiz-Lopez, A., 2021. Impact of dimethylsulfide chemistry on air quality over the Northern Hemisphere. Atmos. Environ. 244, 117961 https://doi.org/10.1016/j.atmosenv.2020.117961.

Zhu, Y., Wang, Y., Zhou, X., Elshorbany, Y.F., Ye, C., Hayden, M., Peters, A.J., 2022. An investigation into the chemistry of HONO in the marine boundary layer at Tudor Hill marine atmospheric Observatory in Bermuda. Atmos. Chem. Phys. 22, 6327–6346. https://doi.org/10.5194/acp-22-6327-2022.